

FIRE Arctic Clouds Experiment



J. A. Curry,^a P. V. Hobbs,^b M. D. King,^c D. A. Randall,^d P. Minnis^e

G. A. Isaac,^f J. O. Pinto,^a T. Uttal,^g A. Bucholtz,^h D. G. Cripe,^d H. Gerber,ⁱ C. W. Fairall,^g
T. J. Garrett,^b J. Hudson,^j J. M. Intrieri,^g C. Jakob,^k T. Jensen,^l P. Lawson,^l
D. Marcotte,^o L. Nguyen,^e P. Pilewskie,^m A. Rangno,^b D. C. Rogers,^d
K. B. Strawbridge,^o F. P. J. Valero,^h A. G. Williams,ⁿ D. Wylie^p

ABSTRACT

An overview is given of the First ISCCP Regional Experiment Arctic Clouds Experiment that was conducted during April–July 1998. The principal goal of the field experiment was to gather the data needed to examine the impact of arctic clouds on the radiation exchange between the surface, atmosphere, and space, and to study how the surface influences the evolution of boundary layer clouds. The observations will be used to evaluate and improve climate model parameterizations of cloud and radiation processes, satellite remote sensing of cloud and surface characteristics, and understanding of cloud–radiation feedbacks in the Arctic. The experiment utilized four research aircraft that flew over surface-based observational sites in the Arctic Ocean and at Barrow, Alaska. This paper describes the programmatic and scientific objectives of the project, the experimental design (including research platforms and instrumentation), the conditions that were encountered during the field experiment, and some highlights of preliminary observations, modeling, and satellite remote sensing studies.

^aUniversity of Colorado, Boulder, Colorado.

^bUniversity of Washington, Seattle, Washington.

^cNASA Goddard Space Flight Center, Greenbelt, Maryland.

^dColorado State University, Fort Collins, Colorado.

^eNASA Langley Research Center, Hampton, Virginia.

^fAtmospheric Environment Service, Downsview, Ontario, Canada.

^gNOAA/Environmental Technology Laboratory, Boulder, Colorado.

^hScripps Institution for Oceanography, La Jolla, California.

ⁱGerber Scientific, Inc., Reston, Virginia.

^jDesert Research Institute, Reno, Nevada.

^kEuropean Centre for Medium-Range Weather Forecasts, Reading, United Kingdom.

^lSPEC, Inc., Boulder, Colorado.

^mNASA Ames Research Center, Moffett Field, California.

ⁿInstitute for Aerospace Research, National Research Council, Ottawa, Ontario, Canada.

^oAtmospheric Environment Service, Egbert, Ontario, Canada.

^pUniversity of Wisconsin—Madison, Madison, Wisconsin.

Corresponding author address: Dr. J. A. Curry, Program in Atmospheric and Oceanic Sciences, University of Colorado, Box 311, Boulder, CO 80309-0311.

In final form 18 June 1999.

©2000 American Meteorological Society

1. Introduction

The FIRE [First ISCCP (International Satellite Cloud Climatology Project) Regional Experiment¹] Arctic Clouds Experiment was conducted during April–July 1998 to study arctic cloud systems under spring and summer conditions. The main goal of the experiment was to examine the effects of clouds on radiation exchange between the surface, atmosphere, and space, and to study how the surface influences the evolution of boundary layer clouds. Observations collected during the field phase of the project will be used to evaluate and improve climate model parameterizations of arctic cloud and radiation processes, satellite remote

¹FIRE is a U.S. national project that is funded primarily by the National Aeronautics and Space Administration (NASA); it includes participation of scientists from Canada, England, and Netherlands.

sensing of cloud and surface characteristics, and understanding of cloud–radiation feedbacks in the Arctic.

The strategy of the FIRE Arctic Clouds Experiment was to use research aircraft to obtain remote and in situ measurements of the properties of clouds and the sea ice/ocean surface. The NASA ER-2 flew at an altitude of 20 km with a suite of remote sensors that can be used to infer the characteristics of the surface and clouds below. Other aircraft, instrumented with in situ and remote sensing instruments, were used to measure radiation fluxes and the physical, optical, and chemical properties of the clouds. The aircraft observations were made over surface-based observational sites in the Arctic Ocean and at Barrow, Alaska.

FIRE's arctic field program interacted closely with the Surface Heat Budget of the Arctic Ocean (SHEBA) project² (Perovich et al. 1999) and the Atmospheric Radiation Measurement (ARM)³ program (Stokes and Schwartz 1994). SHEBA, ARM, and FIRE share scientific objectives that focus on improving simulations of arctic processes in global climate models and improving satellite retrievals of atmospheric state and sea ice conditions in the Arctic. SHEBA emphasizes the surface energy balance and the sea ice mass balance, while ARM is devoted to surface-based observations and modeling of clouds and radiation. The field component of SHEBA focused on an icebreaker ship deployed in the Arctic Ocean and left to drift for a year, which served as a floating science station. ARM provided a number of key surface-based radiometers and remote sensing instruments designed to provide measurements of clouds and radiation at the SHEBA ice station. ARM also operates a duplicate set of instruments at Barrow as part of a decade-long program to monitor clouds and radiation on the north slope of Alaska.

The FIRE program, which has been under way since 1983, is aimed at improving the simulation of clouds and radiation in large-scale models and enhancing satellite cloud retrieval techniques (Randall et al. 1995). FIRE Phase I (1984–89) was designed to address fundamental questions concerning the characteristics of cirrus and marine stratocumulus cloud systems. FIRE Phase II (1989–94) focused on more

detailed questions concerning the formation, maintenance, and dissipation of cirrus and marine stratocumulus cloud systems.

FIRE Phase III commences an investigation of arctic cloud systems. The FIRE Arctic Clouds Experiment, in collaboration with SHEBA and ARM, represents an important broadening of the scientific scope of the FIRE program. This strategic step was motivated by the importance of the Arctic for the global climate system, and an appreciation of how poorly we understand arctic clouds and the energy budget of the arctic surface. The purpose of this paper is to summarize the FIRE Arctic Clouds Experiment field operations and present some preliminary results. Section 2 presents a more thorough description of the project science objectives. Section 3 describes the research platforms and instrumentation. Section 4 provides an overview of the observations. Section 5 provides some preliminary highlights, including some comparisons of model results with the data.

2. Project goals and objectives

The overarching goals of the FIRE Arctic Clouds Experiment are to improve the satellite retrieval of cloud and surface characteristics in the Arctic, and to improve the representation of arctic clouds and radiation in general circulation models. The objective of the FIRE III field experiment is to produce an integrated dataset that

- 1) supports the analysis and interpretation of physical processes that couple clouds, radiation, chemistry, and the atmospheric boundary layer;
- 2) provides in situ data for testing of satellite and ground-based remote sensing analyses; and
- 3) provides initial data, boundary conditions, forcing functions, and test data to support Arctic FIRE modeling efforts.

Motivated by the plans of SHEBA, FIRE, and ARM to mount field experiments in the Arctic, Curry et al. (1996) prepared a review of research prior to 1995 related to arctic clouds and radiation. While this review provides a background for the science objectives of the FIRE Arctic Clouds Experiment, objectives relevant to large-scale numerical weather prediction and climate modeling in the Arctic are reviewed by Randall et al. (1998). Some background on the science issues that motivated the FIRE Arctic Clouds Experi-

²SHEBA is a U.S. national program that is funded primarily by the National Science Foundation (NSF) and the Office of Naval Research (ONR); it includes the international participation of Canada, Japan, and Russia.

³ARM is sponsored by the U.S. Department of Energy (DOE).

ment is given below, as well as specific science questions that focused the scientific investigations.

a. *Clouds*

Substantial uncertainties exist in our present understanding of arctic clouds. These uncertainties arise from difficulties in observing these clouds, both from the ground and from satellite, and from the unusual cloud types that form in the polar regions. These unusual cloud types include ice crystal clouds that reach the surface, commonly referred to as “diamond dust;” convective plumes associated with leads or polynyas (openings in the sea ice); persistent mixed-phase clouds; and multiple layers of thin cloud decks that occur in the statically stable arctic environment. Some key scientific issues relating to arctic clouds follow:

- What is the influence of leads and other open water on cloud properties when large surface–air temperature differences exist?
- How does the extreme static stability and low atmospheric water vapor content of the lower troposphere, especially during winter, affect the flow of energy across the air–sea interface?
- What is the mechanism that leads to the spectacular multiple-layering of summertime cloud systems over the Arctic Ocean?
- How does the transition of low clouds from liquid to crystalline depend on temperature and aerosol characteristics, and how does the springtime transition differ from the autumnal transition?

b. *Radiation*

Clouds are the dominant atmospheric modulators of the arctic radiation climate. Cloud radiative properties depend on the amount of condensed water, the size and shape of the cloud particles, and the phase of the particles (liquid or ice). Recent studies of arctic clouds suggest that over the course of the year clouds have a net warming effect on the surface, while the top-of-the-atmosphere cloud radiative forcing is dominated by the shortwave flux. The radiation environment of the Arctic is complicated considerably by the highly reflective and inhomogeneous snow/ice surface, the complex vertical structure associated with temperature and humidity inversions, low temperatures and humidity, and high solar zenith angles. Key scientific issues related to arctic radiation follow:

- What is the spectral distribution of longwave radiation? In particular, what is the role of the 20- μm

rotation-band “window” region in regulating the surface and atmospheric temperature in the Arctic?

- What are the effects of springtime “arctic haze” on the absorption of solar radiation in polar clouds?
- What is the role of diamond dust in determining the radiation fluxes?
- What are the shortwave radiative effects of the horizontally inhomogeneous stratocumulus clouds over the inhomogeneous, highly reflective snow/ice surface?
- How do the optical properties of the arctic surface vary in response to changes in snow and ice characteristics (including meltponds)?

c. *Aerosols*

It has been hypothesized that the microphysical and optical properties of arctic clouds are particularly susceptible to influence by atmospheric aerosol. The concentration and size distributions of cloud droplets depend in part on the aerosol in the atmosphere, specifically on the cloud condensation nuclei (CCN). The interactions between clouds and aerosol are not simply one way; scavenging by clouds depletes CCN, but aerosol may also be produced and enhanced within the clouds through chemical and physical processes. Ice particle concentrations in clouds may also be affected by aerosol, although this connection is complex and not well understood. The concentration and composition of the ice-forming nuclei (IFN) are hypothesized to be important for determining the phase of arctic clouds, and therefore their impact on the radiation balance. Key questions regarding the aerosols found in the arctic atmosphere follow:

- What is the activity spectra of CCN and how does it vary?
- What are the sizes and composition of CCN, and how and why do they vary?
- How do the CCN distributions interact with the cloud droplet distributions?
- How do processes within arctic clouds modify CCN?
- What is the nature and source of IFN?
- Is it possible for ice particles to form at relative humidities below water saturation, by deposition nucleation?

d. *Remote sensing*

Satellite retrievals of cloud and surface characteristics are hampered by the complex vertical structure of the atmosphere, including temperature and humid-

ity inversions; low temperatures and low water vapor amounts; little visible, thermal, and microwave contrast between the clouds and the underlying surface; heterogeneity of the underlying surface; and the presence of complex cloud types (e.g., mixed-phase clouds, thin multilayered clouds). Specific questions related to satellite remote sensing of arctic clouds include the following:

- How do the vertical variations of cloud and atmospheric properties affect the interpretation of satellite measurements of clouds?
- How well can surface and atmospheric radiative fluxes be reconstructed from satellite-based observations?
- What are the appropriate averaging periods for surface-based cloud observations so they can be meaningfully compared to satellite data? Do these averaging periods vary significantly as a function of cloud height and/or cloud type?
- How accurately can satellites detect the presence of clouds over ice and snow surfaces?
- What is the radiative significance of clouds that are not accurately detected by satellite?

e. Modeling

To meet the objectives of the FIRE Arctic Clouds Experiment, the following modeling activities are being undertaken:

- A variety of 1D and 3D radiative transfer models are being tested using near-instantaneous measurements of the radiation field and the atmospheric parameters that determine the radiation field (e.g., clouds, temperature, aerosol, trace gas concentrations).
- Large eddy simulation (LES) models are being used to develop parameterizations of cloud and boundary layer processes, which eventually can be incorporated into climate models.
- Improved parameterizations of physical processes for climate models are being tested against field observations using single-column models (SCMs). An SCM is a single vertical array of cells from a 3D climate model, the forcing of which may be highly constrained to test individual parameterizations (Randall et al. 1996).
- To help in providing forecast guidance for the Canadian Convair-580 during the field project, the Canadian Mesoscale Compressible Community Model (MC2) was run at 35- and 10-km resolution (Benoit et al. 1997).

3. Experimental design

The FIRE Arctic Clouds Experiment was designed to produce an integrated dataset that

- supports the analysis and interpretation of physical processes coupling clouds, radiation, chemistry, and the atmospheric boundary layer;
- provides in situ data for the testing of satellite and ground-based remote sensing analyses; and
- provides initial data, boundary conditions, forcing functions, and test data to support arctic modeling efforts.

The overall design of the experiment is to combine measurements at the surface, from research aircraft, and from space to address problems of arctic clouds, radiation, and aerosols, including their modeling and remote sensing.

The operational objectives of the FIRE Arctic Clouds Experiment were to make aircraft observations over the SHEBA ship and Barrow during several months of spring and summer. The location and timing of the FIRE Arctic Clouds Experiment were determined by the scheduled operations of the SHEBA experimental site in the Beaufort Sea during October 1997–11 October 1998. The Canadian Coast Guard icebreaker *Des Groseilliers* was deployed in a multi-year ice floe on 2 October 1997, at 75°16.3'N, 142°41.2'W. The thickness of the undeformed multi-year ice at deployment was 1.7–2.0 m. Instrumentation was fully deployed and operational at the site by 30 October. The ARM site at Barrow was fully operational by 19 March 1998, providing a secondary surface site for the experiment. Over the course of the field study, the SHEBA ice camp drifted considerably northwestward (Fig. 1); it was at 78.5°N, 166°W by the end of July 1998.

A key aspect of the experimental design was to design flight plans that economically used the aircraft resources to provide observations over the entire period of spring and summer transitions in arctic cloud and surface characteristics so as to address a multitude of physical process studies and remote sensing and modeling efforts. Four research aircraft were employed during FIRE. Flights were conducted in the immediate vicinity (~50 km) of, and directly over, the SHEBA surface site and the ARM site at Barrow. The three medium-altitude aircraft made measurements spanning the period 8 April–30 July 1998. In addition, during the period 18 May–6 June, the NASA ER-2

flew at an altitude of 20 km above either the University of Washington (UWA) Convair-580 or the NCAR C-130 aircraft. The timing of the aircraft missions, spanning the period from spring to midsummer, was designed to capture the transition between the wintertime boundary layer with predominantly ice clouds to the summertime boundary layer with predominantly liquid clouds, and to capture the onset of the sea ice melt season. This period was also selected as one for which both climate models and satellite remote sensing techniques are in particular need of improvement.

The flight plans of the three medium-altitude aircraft were designed to meet requirements for measuring both the horizontal variability and vertical structure of the atmosphere. Horizontal traverses of 20–200 km were made at various levels above, below, and within cloud; in the boundary layer; and at various altitudes to map the surface using aircraft remote-sensing instruments. Additionally, slow ascents and descents were made to obtain high-resolution vertical profiles using in situ instruments.

The timing of the flights was coordinated with satellite overpasses. The specific satellites of interest included the following:

- *NOAA-12 and -14 Polar-orbiting Operational Environmental Satellites.* Aboard these satellites are the Advanced Very High Resolution Radiometer, which is a 4- or 5-channel radiometer measuring visible and infrared wavelengths, and the Television Infrared Observation Satellite (TIROS) Operational Vertical Sounder (TOVS), which measures incoming radiation in the infrared and passive microwave with 27 channels.
- *Defense Meteorological Satellite Program F12 and F13.* Aboard these satellites are the Special Sensor Microwave/Imager (SSM/I), which is a 7-channel, 4-frequency, linearly polarized passive microwave radiometric system that measures brightness temperatures at 19.35, 22.235, 27, and 85.5 GHz; and the SSM/T2, which measures the brightness temperature near the 183.3 GHz water vapor line and also at 90 and 150 GHz.
- *RADARSAT-1.* Aboard this satellite is a Synthetic Aperture Radar (SAR), which sends pulsed microwave sig-

nals to Earth and processes the received reflected pulses.

The general strategy for FIRE's satellite remote-sensing research is to use the aircraft primarily to evaluate remote-sensing instruments located at the surface and to extend the point observations made at the surface to the larger horizontal scale seen by satellites. The entire time series of surface-based remote-sensing observations can then be used to evaluate and interpret satellite retrievals of cloud and surface characteristics. Coincident surface-based, aircraft and satellite measurements are essential for some validation exercises.

To support the FIRE modeling activities, the FIRE dataset must be readily accessible for modelers to use. To achieve this end, subsets of the data are being packaged so that they can serve as input files to models as well as for model validation. Specific integrated datasets that are being prepared (in collaboration with SHEBA and ARM) include the Integrated Radiative Flux dataset, the Large-Eddy Simulation dataset, and the Single-Column Model dataset.

Details of the surface-based and aircraft observations are described in detail in the subsequent two subsections.

a. Surface observations

An extensive array of instrumentation was deployed at the SHEBA ice camp. Further information on the ship, its track, and instrumentation can be found on the SHEBA Web site (<http://sheba.apl.washington.edu>).

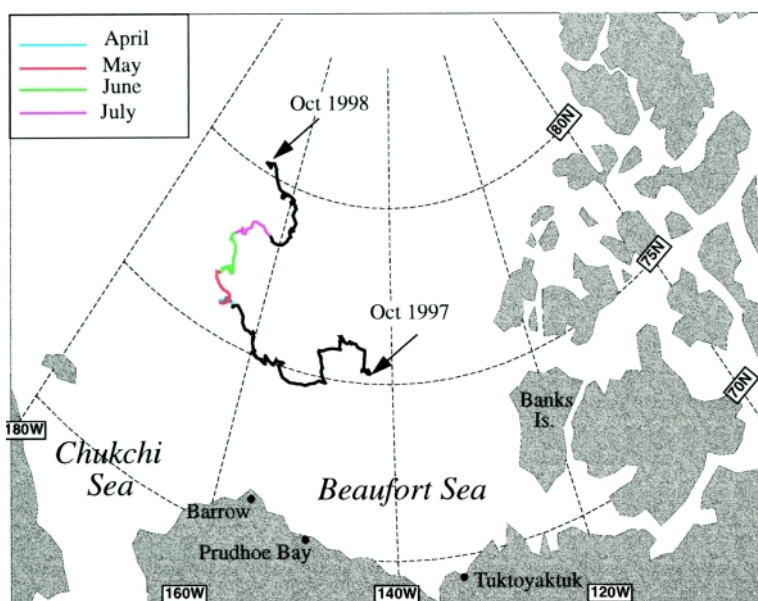


FIG. 1. Map showing drift of the SHEBA ice station.

Information regarding the instrumentation provided by the ARM program can be found on the ARM Web site (<http://www.arm.gov/docs/instruments.html>). The surface-based instrumentation of particular relevance to the FIRE Arctic Clouds Experiment is summarized in Table 1, providing measurements of cloud proper-

TABLE 1. Summary of surface-based measurements at SHEBA.

| <i>Radiation</i> | | |
|---|--|------------------------------|
| Instrument | Wavelengths | Comments |
| Precision/infrared radiometer | broadband (IR) | upwelling and downwelling |
| Precision spectral pyranometer | broadband (SW) | upwelling and downwelling |
| Infrared thermometer | 9.6–11.5 μm | up- and down-looking |
| Normal incidence pyrheliometer | broadband (SW) | direct beam solar irradiance |
| Multifilter rotating shadowband radiometer | 0.415, 0.5, 0.665, 0.862, 0.94 μm | downwelling, direct/diffuse |
| Multifilter radiometer | 0.415, 0.5, 0.665, 0.862, 0.94 μm | upwelling |
| Net radiometer | broadband (SW, IR) | |
| 4- π radiometer | broadband (SW) | deployed on balloon |
| Extended Range Atmospheric Emitted Radiance Interferometer (AERI) | 4–20 μm , 1 cm^{-1} resolution | upwelling |
| Solar Spectral Flux Radiometer (SSFR) | 0.30–2.2 mm, 5–15-nm resolution | zenith, nadir directions |
| <i>Clouds</i> | | |
| Instrument | Wavelengths | Comments |
| Cloud radar | 35 GHz | zenith, up to 13 km |
| Micropulse lidar (DABUL) | 0.5235 mm, polarized | up to 20 km |
| Ceilometer | 0.925 mm | up to 7.5 km |
| Whole sky imager | | cloud fraction |
| Microwave radiometer | 23.8, 31.8 GHz | uplooking |
| Cloud particle replicator | — | deployed on balloon |
| <i>Meteorology and surface fluxes</i> | | |
| Instrument | Wavelengths | Comments |
| GPS rawinsondes | pressure, temperature, humidity, winds | 2–4 times per day |
| Tethered balloon profiles | pressure, temperature, humidity, winds | up to 1 km |
| Vaisala thermistor probe | mean air temperature | on tower, 0–15 m |
| Vaisala hygrometer probe | mean air humidity | on tower, 0–15 m |
| R.M. Young propellor, vane | mean wind velocity | on tower, 0–15 m |
| Setra barometer | air pressure | on tower, 0–15 m |
| Sonic anemometer/thermometer | stress, sensible heat flux | on tower, 0–15 m |
| Ophir rapid response hygrometer | sensible heat flux | on tower, 1 m |

ties and radiation fluxes, meteorological conditions, and the near-surface atmospheric boundary layer.

Incident shortwave and longwave radiation fluxes at the surface were measured by the ARM program, as well as by SHEBA and FIRE investigators. Measurements of the direct solar beam and diffuse solar radiation were also made. Upwelling radiation fluxes were measured, as well as infrared measurements of the skin surface temperature. High-resolution spectral measurements were made in both the solar and infrared portions of the spectrum, which can be used to retrieve atmospheric temperature and humidity profiles, trace gases, aerosol characteristics, and cloud properties.

Cloud properties were measured at the SHEBA site using ground-based remote sensors and a tethered balloon. Remote measurements were made almost continuously for the duration of the SHEBA deployment. The cloud radar, lidar, and ceilometer are used to determine cloud layer boundaries and cloud fraction. Cloud microphysical properties such as liquid and ice water content and particle phase and size are determined from retrievals using the cloud radar, lidar, microwave radiometer, and other radiometers such as the AERI and SSFR. To obtain in situ measurements of cloud properties, tethered balloons with instruments for cloud microphysical and radiation measurements were flown between March and June. Instruments flown on the balloons measured profiles in the lowest 1 km of the atmosphere of cloud particle concentrations and size distributions, and mean radiative intensities (actinic flux).

Meteorological data were obtained from rawinsondes, tethered balloon profiles up to 1 km, and measurements from several towers (10–20 m in height). Turbulent fluxes of sensible and latent heat and mo-

mentum were obtained at multiple levels from the 20-m tower.

SHEBA investigators conducted detailed measurements of the optical and physical characteristics of snow and sea ice, including snow depth, density, and grain size, as well as ice temperature, salinity, density, brine volume, and air volume. Studies were also conducted over lines ranging up to 20 km in length to assess the spatial variability of snow characteristics, surface albedo, and ice transmittance.

Observations of atmospheric state, cloud characteristics, and radiation fluxes using nearly identical instruments to those at SHEBA were obtained at the ARM site in Barrow, Alaska, beginning 19 March 1998.

b. Aircraft observations

Four research aircraft were deployed during the FIRE Arctic Clouds Experiment: the NASA ER-2, the National Center for Atmospheric Research (NCAR) C-130Q, the UW Convair-580, and the Canadian National Research Council Convair-580 (Table 2). Summaries of the remote sensing and cloud microphysical instrumentation deployed on these aircraft are given in Tables 3 and 4.

The NASA ER-2 is a single-engine, single-seat, high-altitude subsonic aircraft. Active and passive remote-sensing instruments were deployed on the ER-2 during this period, to determine properties of clouds, aerosols, trace gases, surface temperature, cloud and surface radiation characteristics, sea ice concentration and age, precipitation, and profiles of temperature, water vapor, and ozone. A summary of the remote sensing instrument characteristics and derived data products is given in Table 3. Details of the instruments on the ER-2 can be found on the FIRE Arctic Clouds

TABLE 2. Overview of aircraft platforms.

| Aircraft | Altitude (ft) | Base | Flight Period (1998) | No. of flights over SHEBA | No. of flights over Barrow |
|----------------------|---------------|-----------|------------------------------|---------------------------|----------------------------|
| NASA ER-2 | 60 000 | Fairbanks | 18 May–6 Jun | 8 | 11 |
| NCAR C-130Q | 100–25 000 | Fairbanks | 4 May–27 May 8 Jul–30 Jul | 8 8 | 0 0 |
| UW Convair-580 | 50–32 000 | Barrow | 19 May–24 Jun | 8 | 11 |
| Canadian Convair-580 | 50–25 000 | Inuvik | 8 Apr–29 Apr | 4 | 2 |

TABLE 3. Airborne remote-sensing instrumentation. Swath width and pixel size are determined for typical aircraft flight levels (20 km for the ER-2; 4 km for the C-130).

| Sensor | Wavelengths | Scanning mode | Pixel size | Data products |
|--|--|------------------|-------------|--|
| NASA ER-2 | | | | |
| Modis Airborne Simulator (MAS) | 0.47–14.3 μm 50 bands | cross track | 50 m | solar spectral radiance bidirectional reflectance cloud particle phase and size, optical depth |
| Millimeter-wave Imaging Radiometer (MIR) | 89, 150, 183.3 \pm 1, 183.3 \pm 3, 183.3 \pm 7, 220, 340 GHz | cross track | 1 km | surface emissivities cloud ice water path water vapor profiles |
| Advanced Microwave Precipitation Radiometer (AMPR) | 10.7, 19.35, 37.1, 85.5 GHz | cross track | 0.65–2.8 km | surface emissivities cloud liquid water path, rainfall sea ice concentration, age |
| Cloud Lidar System (CLS) | 1064, 532 nm | nadir | | cloud boundaries vertical structure |
| High-Resolution Infrared Spectrometer (HIS) | 3–17 μm 0.5 cm^{-1} resolution | nadir | 2 km | surface temperature profiles of T , $\text{H}_2\text{O}(g)$, O_3 cloud height, emissivity particle size and phase |
| Solar Spectral Flux Radiometer (SSFR) | 300–2200 μm 5–15-nm resolution | zenith, nadir | | reflectance and transmissivity surface spectral albedo cloud phase, optical depth |
| Airborne Multiangle Scanning Radiometer (AirMISR) | 433, 555, 670, 865 nm | nine look angles | | cloud-top geometry |
| NCAR C-130 | | | | |
| Radiation Measurement System (RAMS) | solar (direct/diffuse), IR | zenith, nadir | hemispheric | solar and IR fluxes albedo, optical depth |
| Airborne Imaging Microwave Radiometer (AIMR) | 37, 90 GHz | | 70–180 m | cloud liquid water path, rainfall sea ice concentration, age |
| Multispectral Channel Radiometer (MCR) | 0.63, 0.761, 0.763, 1.06, 1.64, 2.16, 10.8 μm | cross track | 28 m | cloud fraction, optical depth particle size and phase |

TABLE 3. Continued.

| Sensor | Wavelengths | Scanning mode | Pixel size | Data products |
|---------------------------------------|---|---------------|------------|--|
| UW Convair 580 | | | | |
| Cloud Absorption Radiometer (CAR) | 13 wavelengths 470–2300 nm | scanning | | absorption, scattering of SW bidirectional reflectance |
| Solar Spectral Flux Radiometer (SSFR) | 300–2200 nm 5–15-nm resolution | zenith, nadir | | bidirectional reflectance cloud phase, optical depth |
| Canadian Convair 580 | | | | |
| Lidar | 1.064 μm polarization | nadir, zenith | | backscatter, depolarization ratio cloud height, particle shape |
| Landsat simulator | 504–597, 598–700, 702–798, 805–1042 nm | scanning | | |

Experiment Web site (<http://eosweb.larc.nasa.gov/ACEDOCS/data/appen.d.2.html>).

The three medium-altitude aircraft shared some common instrumentation. In particular, many of the instruments to measure in situ cloud microphysical and aerosol characteristics were common to all three aircraft. Parameters measured by these aircraft include aerosol concentration, composition and size distribution, cloud particle concentration and size distribution, liquid water content, droplet effective radius, particle shape, cloud condensation nuclei spectra, and ice nucleus concentration and composition. Specific cloud physics and aerosol instruments are listed in Table 4.

The NCAR C-130Q is a four-engine, medium-altitude research aircraft that is designed to carry a payload of up to 13 000 lbs with full fuel load. The NCAR C-130Q measures atmospheric state parameters, turbulent fluxes, cloud physics, and radiative fluxes, and also conducts remote sensing using scanning radiometers and video photography. In addition to the NCAR instruments, the C-130Q can support a large user-supplied payload. Some of the major research instrumentation deployed on the C-130Q for this experiment is described in Tables 3 and 4.

The UW Convair-580 is a two-engine, medium-altitude research aircraft, which flew research missions for the first time in this experiment but deployed instrumentation that has been used frequently by the UW on other aircraft. The UW Convair-580 measures atmospheric state parameters, cloud physics, radiative fluxes, and aerosol chemistry, and includes remote-sensing instrumentation (see Tables 3 and 4).

The Canadian Convair-580 aircraft is nearly identical to the UW Convair-580. The Canadian aircraft measured atmospheric state parameters, turbulent fluxes, cloud physics, radiative fluxes, and aerosol and air chemistry. Trace gas measurements included O_3 , SO_2 , and organohalogens, as well as fast response humidity and CO_2 measurements. Aerosol chemistry included total organic carbon, speciated organics, inorganic and organic ions, black carbon, trace metals, and total organic carbon.

4. Overview of experiment

The operational objectives of the FIRE Arctic Clouds Experiment were to make aircraft observations over the SHEBA ship during several months of spring and summer, using Fairbanks, Alaska; Barrow,

TABLE 4. Cloud microphysical and aerosol instruments on the medium-altitude aircraft: NCAR C-130 (C-130), UW Convair 580, and Canadian Convair 580 (CAN).

| Instrument | Parameter | Range | C-130 | UW | CAN |
|---|--|---|-------|----|-----|
| Passive cavity aerosol spectrometer probe PCASP-100 | aerosol size distribution | 0.1–3.0 μm (diameter) | x | x | x |
| Condensation nucleus particle counter | total aerosol concentration | | x | x | x |
| Forward scattering spectrometer probe FSSP-300 | size and concen of aerosol and drops | 0.3–20 μm (diameter) | x | x | x |
| FSSP-100 | cloud drop size distribution and concentration | 2–47 μm (diameter) | x | x | x |
| Scanning humidigraph | effect of RH on aerosol light scattering | 30% < RH < 85% | | x | |
| Laser aerosol spectrometer-200 | aerosol size distribution | 0.5–11 μm | | x | |
| Differential mobility particle spectrometer | aerosol size distribution | 0.01–0.6 μm | | x | |
| 1D optical array probe (OAP) 260X cloud probe | drop and crystal size distribution | 40–600 μm (length) | x | x | x |
| 2D OAP cloud probe | drop and crystal shape and size distribution | 25–800 μm (length) | x | x | x |
| 2D OAP precipitation probe | rain and snow particle shape and size distribution | 200–600 mm (length) | x | | x |
| 2D OAP Grey probe | particle shape and size distribution | 25–1600 μm | | | x |
| SPEC cloud particle imager (CPI) | digital images of cloud particles | 5–2300 μm | x | x | x |
| Cloudscope | mass and size distribution of ice particles | | x | | x |
| DRI replicator | images of cloud particles | | | | x |
| King Hot-wire Probe | liquid water content | 0.05–3 g m^{-3} | x | | x |
| Johnson–Williams Probe | liquid water content | 0–2 g m^{-3} | x | x | |
| Gerber PVM-100A | liquid water content drop effective radius | 0.05–3 g m^{-3} | x | x | |
| Icing detector | supercooled liquid water content | 0.001–1 g m^{-3} | x | | x |
| Nevzerov probes | liquid water content | | | | x |
| Counterflow virtual impactor (CVI) | condensed water content in-cloud aerosol char | impacts cloud part d = 5–30 μm | | | x |
| Cloud condensation nucleus spectrometer | CCN spectra | supersaturation range 0.01%–2% | x | | x |
| Continuous flow diffusion chamber (CFD) | concentration and composition of IFN | | x | | |
| Integrating nephelometer | aerosol backscattering coeff | | | x | x |
| Particle soot-absorption photometer | light absorption, graphitic carbon | | | x | |
| Cloud integrating nephelometer | scattering/extinction coeff asymmetry parameter | 635 nm | | x | |

Alaska; and Inuvik, Northwest Territories, as bases of operation. The SHEBA ship, initially deployed at 75.27°N, 142.69°W, was expected to drift to the west-northwest about 320 n mi by the end of the experiment (based upon buoy drift over the past 20 years). By the commencement of the Canadian Convair flights in April, the ship had moved to 76.12°N, 164.64°W, which was beyond the range of the Canadian Convair based in Inuvik. Hence, it was necessary for the Canadian Convair to refuel and over-night in Barrow when making flights to the SHEBA ship. During July, the ship was located in the vicinity of 78.11°N, 167.16°W, which required a one-way ferry time of 3 h for the C-130Q from Fairbanks, significantly diminishing flight time on station. The UW Convair, based in Barrow, was in the best position to reach the SHEBA ship; nevertheless the SHEBA ship was 410 n mi from Barrow by the end of its flights in June.

Communications from the ship to the mainland were handled by INMARSAT, which advertises communication only as far as 75°N. As the ship continued to drift northward, concerns were raised that the ship would lose satellite communication, but this did not happen. All four aircraft were able to communicate with the ship via high-frequency radio when they were within about 100 mi of the ship. This communication was extremely valuable in conducting the flights, since updates from the surface-based observations and satellite observations received on the ship via TERASCAN allowed modification of flight patterns to optimally sample the situation.

An additional consequence of the large westward shift of the SHEBA ship was that it left the Beaufort Sea (the original targeted region for the measurements) by the end of winter and moved into the Chukchi Sea (see Fig. 1). The Beaufort Sea is characterized in summer and spring by a surface anticyclone and a predominance of stratus clouds. In the Chukchi Sea, the weather situation was more dynamic with southerly flow predominating during June and July, bringing in high clouds that were often associated with frontal systems. Because the SHEBA ship was often on the edge

of the anticyclone or affected by small storms, forecasting the weather for flight operations was difficult, particularly during July, with conditions often changing rapidly. The difficulty in forecasting the weather, combined with the long ferry flight to the SHEBA ship, made it difficult to plan flights prior to actually receiving radio communication from the ship about an hour before arriving at the site.

Table 5 gives an overview of the conditions sampled by the three medium-altitude research aircraft during the FIRE Arctic Clouds Experiment. A variety of conditions were sampled, including clear skies, boundary layer clouds, mid- and upper-level clouds, and clouds in the presence of open leads. Various flight patterns were flown, aimed at evaluating surface-based, satellite, and ER-2 remote sensing instruments, and providing input for evaluating and modeling cloud–radiative interactions, boundary layer clouds, surface albedo and radiation fluxes, and surface characteristics. Given the limited number of flight hours and temporal coverage of the aircraft flights, we were

TABLE 5. Distribution of cases (expressed as number of flights) for medium-altitude aircraft: NCAR C-130 (NCAR), UW Convair 580, and Canadian NRC Convair 580.

| | No. of Cases | | | |
|--|--------------|----|-----|-------|
| | NCAR | UW | CAN | Total |
| <i>Cloud conditions</i> | | | | |
| Clear | 2 | 1 | | 2 |
| Open leads | 0 | 0 | 8 | 8 |
| Cloudy boundary layers | | | | |
| liquid | 4 | 10 | 3 | 17 |
| ice | | | 1 | 1 |
| mixed phase | 3 | 7 | 6 | 16 |
| Cirrus and altostratus | 6 | 4 | 9 | 15 |
| Storm (precipitation) | 2 | 1 | 3 | 6 |
| <i>Flight patterns</i> | | | | |
| Mapping of surface features | 15 | | | 15 |
| Surface albedo and radiation fluxes | 14 | 8 | | 22 |
| Validation of surface remote sensing instruments | 13 | 14 | 6 | 33 |
| Cloud radiative properties | 14 | 8 | 4 | 28 |
| Cloudy boundary layer | 7 | | 8 | 15 |
| Bidirectional reflectance | | 15 | | 15 |

not able to sample with aircraft the entire range of weather and cloud conditions that occur in this locale. Because of high winds during July, we obtained only one case of a statically stable summertime arctic stratus, and none with multiple cloud layers in the boundary layer. We also did not obtain as many cases where there was only ice (no liquid) in the atmosphere as would have been optimal for both modeling and remote-sensing studies. Nevertheless, the cases sampled provide a rich dataset with which to address the project objectives.

During the period of aircraft measurements (April–July 1998), cloud and surface conditions over the ice changed from near-winter conditions with boundary layer ice clouds and a snow-covered surface, to the peak of the summer melt season with abundant meltponds and liquid clouds in the boundary layer. An overview is given below of the weather, cloud, and surface characteristics at the SHEBA ship for each of these four months.

a. April

At the beginning of the Canadian Convair-580 flights on 8 April, the surface air temperature at SHEBA was -13°C ; at the end of the flights on 29 April it was -18°C . During mid-April there was a 4-day period when the surface air temperature remained unseasonably warm, above -10°C . Boundary layer clouds sampled in the vicinity of the ship were entirely liquid on 17 April, when cloud temperatures were -5° to -10°C , and entirely crystalline on 21 April when cloud temperatures were -15° to -20°C . The synoptic situation in April was dominated by a surface high northeast of the ship with a broad weak cyclone in the lower Chukchi Sea and along the Alaskan coast. This combination produced easterly surface winds most of the time with southerly or southeasterly winds aloft. Deviations occurred when a cyclone moved north out of the Bering Strait, crossing the SHEBA ship on 18–21 April, and a surface anticyclone invaded from the northwest during 24–26 April. Some of the Canadian flights took place close to the coast between Inuvik and Barrow, and included sampling of open water regions associated with leads and polynyas.

b. May

During May 1998, the C-130Q, ER-2, and UW aircraft conducted research flights. May was dominated by an anticyclone to the east of the ship that moved north later in the month. A persistent cloud-

topped surface mixed layer was present from 30 April through 19 May. Surface-based mixed layers are thought to be rare in the Arctic, although they are most likely to occur during May when the surface warms rapidly. At the SHEBA ship, steady warming at the surface was evident, with temperatures of -20°C at the beginning of the month and 0° to 2°C at the end of the month. Early in the month, two leads opened in the vicinity of the SHEBA ship, several hundred meters wide. These leads froze and reopened intermittently during the month, but during the latter half of the month virtually no open water could be seen in the vicinity of the SHEBA ship. At the end of the month, snowmelt began, which was accelerated by several days of rain.

c. June

June weather was characterized by an anticyclone east of the SHEBA ship, which moved into Canada on occasion. The ship was generally under a southerly flow caused by weak cyclones and upper-air troughs to the west. During the first week of June, a near balance existed between upwelling and downwelling longwave radiation at the surface; however, the net shortwave radiation of about 150 W m^{-2} near solar noon contributed significantly to snowmelt and the development of meltponds. Clouds were clearly warming the surface; during clear-sky periods the net radiation became negative and the surface changed from melting to freezing. The surface melting was somewhat sporadic, interrupted by periods of surface freezing induced by clear skies and/or high surface winds. By the third week in June, most of the snow had melted. During June, multilayered clouds were most commonly encountered, with the bases and tops of a given layer varying appreciably over relatively short distances.

d. July

July was a fairly stormy month, with persistent southerly flow from the North Pacific Ocean and frequent mid- and high-level clouds. A strong surface temperature inversion characterized the region from 17 to 30 July, the strength of the surface inversion reaching as high as 12°C . Periodically, a shallow, surface-based mixed layer less than 100 m deep would develop under conditions of high wind speeds or a surface fog, especially during the first half of the month. Boundary layer clouds were entirely liquid in phase. Surface characteristics evolved over the course of the month, with increased meltpond coverage and open water, and corresponding decreases in surface albedo.

5. Some highlights of preliminary results

In this section we present some examples of data collected in the FIRE Arctic Clouds Experiment that illustrate the technology used in the experiment and how the datasets can be synthesized and integrated to help improve modeling and satellite remote sensing and to address key scientific questions.

a. Clouds

Among the numerous cloud situations observed during the experiment, we describe here two cases that illustrate the data and some preliminary findings on cloud particle phase.

Measurements of cloud characteristics are illustrated for 4 May using C-130Q and surface-based observations. The time series of cloud radar returns (see Fig. 2) shows a persistent boundary layer cloud (-10 dBZ) surmounted by altostratus clouds (-40 dBZ) that had almost disappeared by 2200 UTC when the C-130Q arrived on site. The boundary layer was characterized by a cloud-topped mixed layer (Fig. 3), with cloud top at 1080 m and base at 660 m. The humidity inversion above the cloud-topped mixed layer appears to have contributed to the homogeneity and persistence of the cloud deck by inhibiting evaporative cooling associated with entrainment mixing at cloud top. Such humidity inversions are rare outside the polar regions; they are hypothesized to be associated with moisture advection and precipitation drying of the lower atmosphere (by diamond dust, snowfall, and drizzle). Profiles of liquid and ice water content (Fig. 3c) show that the cloud was mixed phase, with slightly more than half of the condensed water in the crystalline phase. This is consistent

with the enhanced lidar backscatter values in Fig. 2b between 660 and 1100 m, indicating the presence of liquid water. The ice water content in Fig. 3b was determined from the Cloud Particle Imager (CPI), using images such as those shown in Fig. 4. Also determined from the CPI are size spectra of the ice particles (Fig. 4). CPI images taken above the cloud show rosettes greater than $500 \mu\text{m}$, columns with side plane growth and small ice particles; presumably these particles have fallen from the dissipating altostratus cloud. These large particles accreted drops as they fell through the mixed-phase cloud and probably account for the presence of relatively large (up to 1 mm) rimed

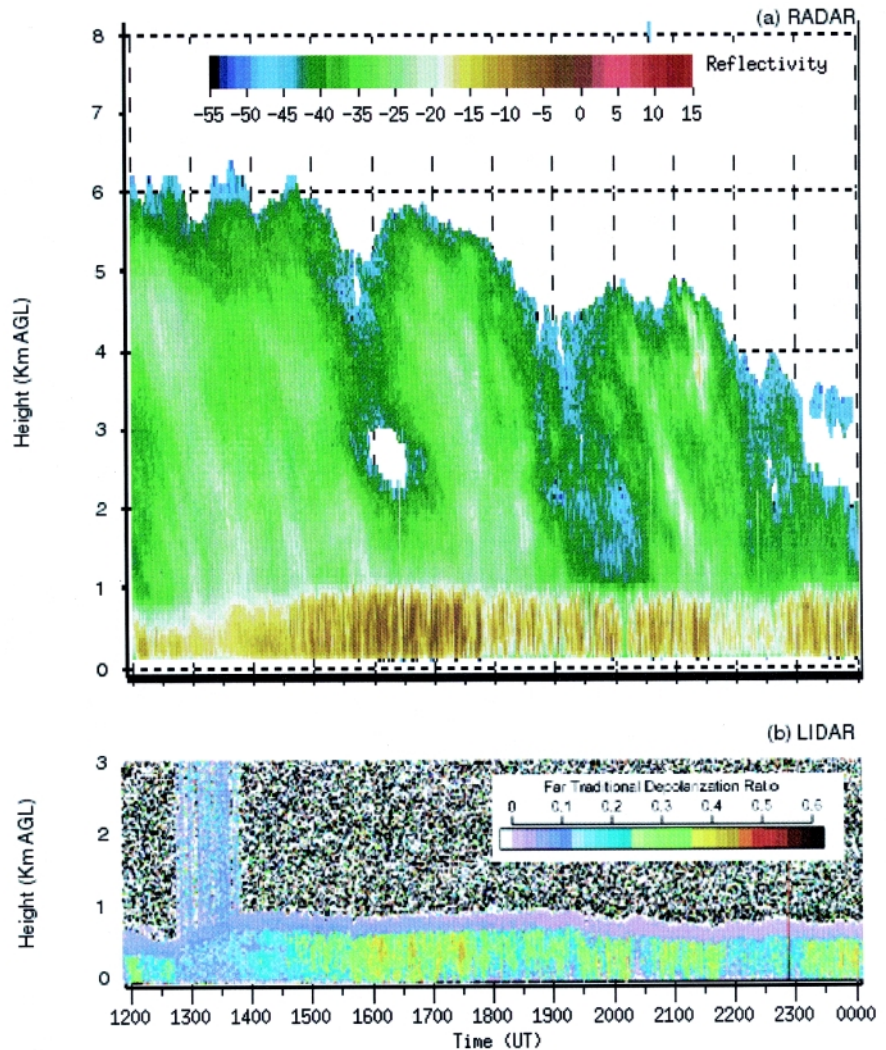


FIG. 2. Time series of (a) cloud radar and (b) lidar depolarization observations from the SHEBA ship for 4 May 1998. In (a), the lidar reflectivity shows a boundary layer cloud at altitudes below about 1 km with reflectivity of about -10 dBZ, and an altostratus cloud (about -40 dBZ) at higher levels that was gradually diminishing with time. In (b), the lidar is attenuated by liquid water at altitudes above about 800 m, with depolarization ratios less than 0.2 indicating the presence of liquid water.

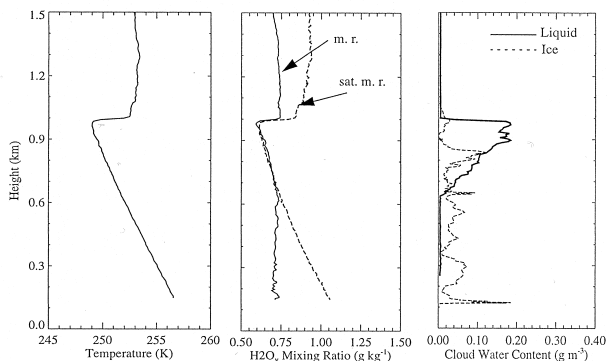


FIG. 3. Vertical profile of the cloudy boundary layer on 4 May 1998 at 2300 UTC from the NCAR C-130Q. (a) Temperature; (b) water vapor mixing ratio; (c) liquid water content (solid line) determined by the King probe and ice water content (dashed line) determined from the Cloud Particle Imager (CPI).

ice particles in this shallow cloud. The regions with large rimed particles also account for the peaks in the ice water content (Fig. 3c). Below cloud, precipitation in the form of mostly rimed ice particles was observed. Near the SHEBA ship, ice forming nucleus (IFN)

concentrations were quite small, less than 0.5 L^{-1} at -22°C at a water supersaturation of 3%. Above cloud top the IFN concentration was $\sim 25 \text{ L}^{-1}$ at -27°C . Condensation nuclei (CN) at low levels were fairly low and uniform ($\sim 200 \text{ cm}^{-3}$), indicating relatively clean air.

One of the unusual cloud types that occur over sea ice during the cold portion of the year is convective clouds that emanate from open water in leads or polynyas. Figure 5 depicts a low-level transect by the Canadian Convair 580 aircraft across Cape Bathurst Polynya in the Beaufort Sea (near 70°N , 135°W) on 25 April 1998. The lowest panel shows output from a downward-looking multispectral Landsat spectrometer in the wavelength interval $0.45\text{--}0.52 \mu\text{m}$ with a 15° field of view. Clearly evident is the sharp transition from solid sea to open water on the southern edge of the polynya (point A), with thin ice and leads (between points B and C) characterizing the region to the north of the polynya. The upper two panels show ambient temperatures and humidities along the transect and eddy correlation fluxes of the same quantities.

Advection of cold air over the relatively warm open water resulted in positive sensible heat and moisture fluxes between points A and B, leading to increases in potential temperatures and specific humidities in the downwind direction across the polynya. The sensible and latent heat fluxes resulted in the formation of a shallow convective cloud over the polynya that is advected downwind (Fig. 6) on 27 April.

Large variations in the relationship between cloud temperature and phase of the arctic clouds were seen in this experiment, consistent with previous observations (e.g., Curry et al. 1996; Hobbs and Rangno 1998). During May, liquid water was observed by the C-130Q in mixed-phase clouds at temperatures as low as -23°C , while during June the UW Convair-580 observed ice crystals in mixed-phase clouds at temperatures as high as -4°C . In the ab-

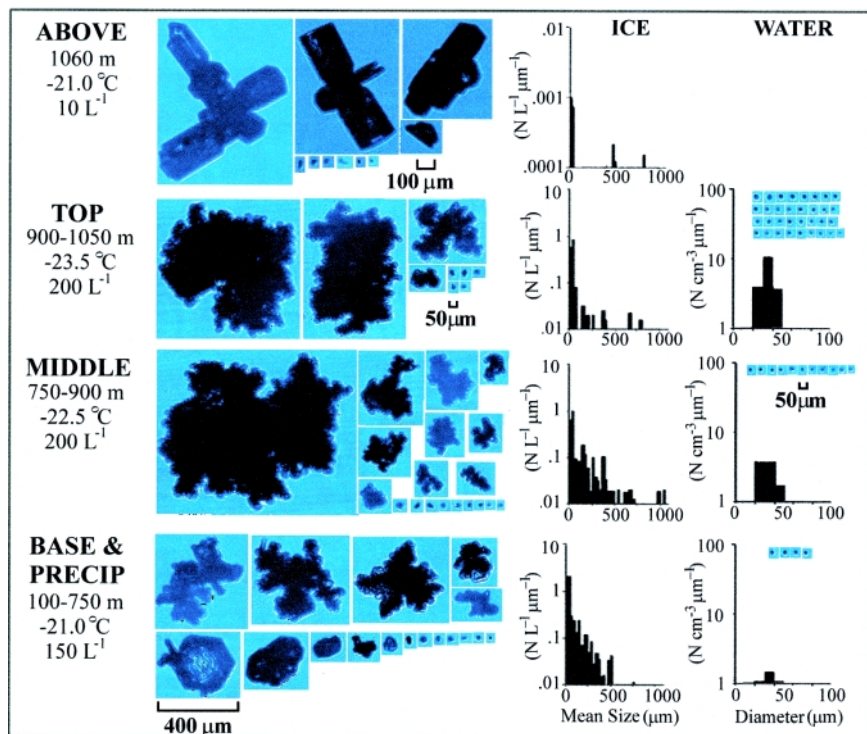


FIG. 4. Observations of cloud particles from the CPI aboard the C-130Q on 4 May 1998. Profile segment heights, average temperatures, and average particle concentrations are listed at the left for above cloud top, just below cloud top, in middle of cloud, and in the precipitation region. Representative images of ice particles (middle left) and water drops (right) are shown for each profile segment. Size distributions for ice particles (middle right) and water drops (right) are averaged over a time period for each profile segment.

sence of ice particles falling from above, such as the case in Fig. 4, the occurrence of ice in the boundary layer clouds appears to be related to maximum droplet sizes. For example, ice crystals were present between -4° and -6°C when the cloud droplets were large ($> 25\ \mu\text{m}$ diameter, also typically some drizzle drops present) and in concentrations of at least a few per cubic centimeter. Overall cloud droplet concentrations were low ($< 100\ \text{cm}^{-3}$) in these cases as well. Conversely, colder boundary layer clouds (down to around -12°C) with smaller cloud droplets generally did not contain ice. Also, overall cloud droplet concentrations were higher ($> 100\ \text{cm}^{-3}$) in these cases. These observations support the picture presented by Hobbs and Rangno (1998).

b. Aerosols

During the FIRE Arctic Clouds Experiment, the atmosphere was frequently pristine near the surface. However, haze layers several hundreds to thousands of meters thick were common aloft, indicating long-range transport. Figure 7 shows an example of a vertical profile flown by the UW Convair-580 through a thick haze layer that probably originated in Asia. Tenuous cirrostratus cloud was present above 5 km; at 100-m altitude there was a very thin (16 m) stratus layer. The profiles shown in Fig. 7 show relatively high values of extinction and scattering at altitudes exceeding 4000 m, and the haze layer shows considerable structure. The extinction coefficient has at least eight distinct maxima over the depth of the profile. Furthermore, within each maximum there are varying degrees of absorption, suggesting differing sources and/or aging of the aerosol.

Within 100 m of the surface, Fig. 7 shows that extinction and scattering were very low. Accumulation-mode particle concentrations were 10 times greater aloft than at the surface. Precipitation scavenging of these particles by boundary layer stratus may have created these unusually clean conditions near the surface. During May, the NCAR C-130Q generally observed very low concentrations of CN, CCN (cloud condensation nuclei), and IFN in the boundary layer, indicating a very clean background and fairly efficient or long-duration scavenging mechanisms. The CN values of $\sim 10\ \text{cm}^{-3}$ for extended periods are among the cleanest in the world. Occasionally during May, the C-130Q observed small-scale regions near the surface with high concentrations of aerosol particles, particularly IFN, possibly associated with open water in leads. It has been hypothesized that ocean bacteria may be

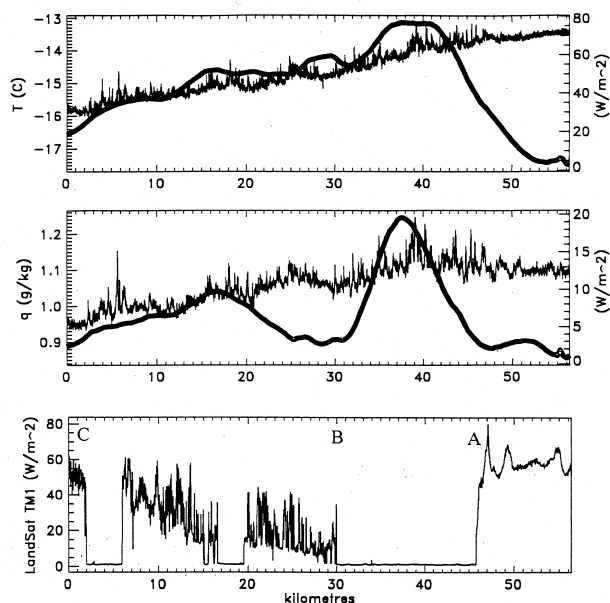


FIG. 5. Data obtained from a transect flown at 300-m altitude by the Canadian Convair-580 aircraft across Cape Bathurst Polynya in the Beaufort Sea ($70^{\circ}12'\text{N}$, $134^{\circ}45'\text{W}$) on 25 April 1998. The polynya is shown in (c) between points A and B: (a) air temperature (thin) and its vertical turbulent flux (bold), (b) specific humidity (thin) and its vertical turbulent flux (bold), (c) reflected solar radiation flux in the wavelength interval $0.45\text{--}0.52\ \mu\text{m}$.

active as ice nuclei, but it is not clear how these could enter into the atmosphere from the small areas of open water in the Arctic Ocean.

During July, very high concentrations of small aerosol particles were observed from the C-130Q in the boundary layer. Volatility tests suggest that the particles were sulfuric acid, which is consistent with local production of dimethyl sulfide in the Arctic Ocean during the melt season (Ferek et al. 1995). Local production of aerosols was also observed in the humidity inversion above boundary layer clouds and also in dissipating cloud layers. In about 30% of the cloudy boundary layer cases sampled by the UW Convair-580, the total particle concentrations in a layer just above the top of the cloud layer were $\sim 1000\ \text{cm}^{-3}$ (in some cases $8000\ \text{cm}^{-3}$) greater than those immediately above or below the layer. The cases with enhanced particle concentrations above cloud top were associated with a cloud-top temperature and a humidity inversion (e.g., see Fig. 3). Nucleation-mode particles may have been responsible for the increases in total particle concentration, possibly formed by gas-to-particle conversion in the layer of enhanced humidity. A similar phenomenon was observed from the

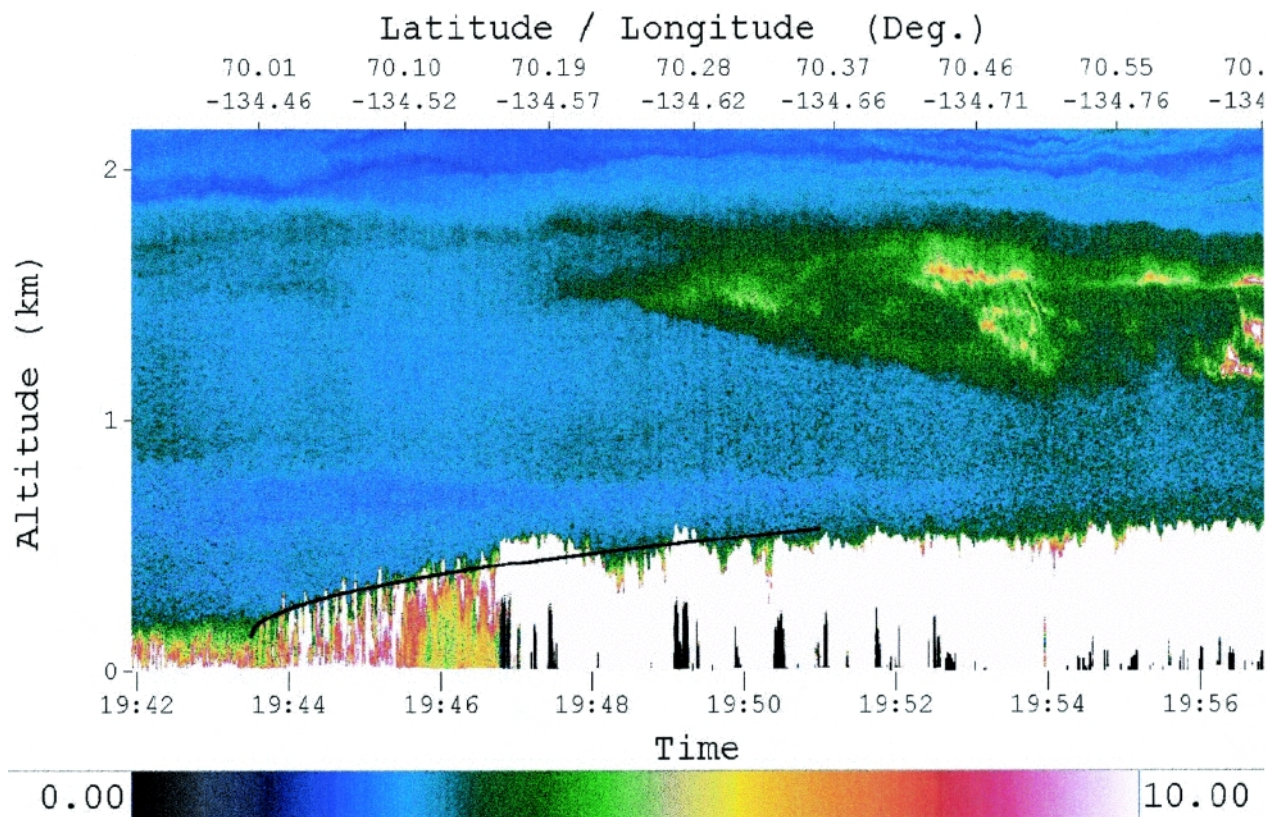


FIG. 6. Observations from the downward-pointing lidar aboard the Canadian Convair-580 on 27 April 1998, across the Cape Bathurst Polynya in the Beaufort Sea (near 70°N, 134.5°W). The upwind edge of the polynya is near the left edge of the figure. The scale bar represents backscatter ratio (no units) from 0 to 10, indicating the amount of scatter relative to “clear” air. The cloud plume is shown by the highest backscatter values. The growth of the internal boundary layer over the polynya is indicated by the solid line.

C-130Q. In some cloud layers, even after the clouds had dissipated, enhanced CN (but not IFN) were observed, presumably associated with particle production by gas-to-particle conversion in the humid air.

On 14 June, between 1950 and 2130 UTC, the UW Convair-580 aircraft flew a series of three horizontal transects through the lower, middle, and upper portions of a uniform stratus cloud about 200 m thick. The transects were flown from 43 km downwind of Barrow (point A) to 129 km downwind of Barrow (point B). Transects flown below the cloud and in the cloud showed a clear gradient in interstitial CN concentrations, with concentrations highest closest to Barrow. These measurements point to the advection and dispersion of an anthropogenic plume downwind of Barrow. The effects of particle emissions from Barrow on the microstructure of the stratus cloud was readily apparent. Mean droplet concentrations in the vicinity of A and B were 68 and 25 cm^{-3} , respectively. The mean values of the cloud droplet effective radius at A and B were 9.5 and 11.1 μm , the mean drizzle fluxes at A and B were 0 and 1.7 mm day^{-1} , and the mean

liquid water contents at A and B were 0.18 and 0.15 g m^{-3} , respectively. Thus, the Barrow plume increased droplet concentrations in the stratus, decreased cloud droplet effective radius, and effectively shut off drizzle. These observations highlight the sensitivity of the arctic stratus clouds to modification by anthropogenic aerosol.

c. Radiation

Numerous radiometers on the aircraft and at the surface provide a detailed picture of the radiation environment in the vicinity of the SHEBA ship. Here we describe some elements of the surface and cloud radiation characteristics.

The evolution of area-average surface albedo (obtained from the ratio of the upwelling to downwelling broadband solar flux) in the vicinity of the SHEBA ship, measured by the UW Convair-580 and the NCAR C-130Q, is shown in Fig. 8. During May, the average surface albedo values for the six NCAR C-130Q flights where the surface could be observed ranged from 0.85 to 0.67. No change was obvious in

amounts of open water or new ice. The highest albedo (0.85) was measured on 18 May after a fresh snowfall beneath an optically thick liquid cloud. The lowest value of 0.67 was measured under a clear sky on 20 May. On 29 May, the first rainfall of the season caused melt metamorphism to begin and the first surface melt ponds began forming during the first week of June. The largest gradient in surface albedo occurred during the period 7–18 June, when most of the snowmelt occurred. By 18 June, most of the surface snow had disappeared. Area-averaged surface albedos in the vicinity of the ship ranged from 0.42 to 0.56 during July, depending on the evolution of the surface melt and the cloud characteristics. Surface albedo was strongly influenced by cloud optical depth. On 18 July, we determined a totally diffuse surface albedo of 0.56 in the vicinity of the ship under heavy overcast. Just east of the ship under clear-sky conditions, with no obvious differences in surface features, the surface albedo was 0.40.

During April and the first half of May, considerable inhomogeneities in upwelling radiation were seen, associated with ice of different thickness and also open water. Figure 9 shows a time series of hemispheric upwelling shortwave and longwave radiation obtained on 7 May from the C-130 at an altitude of 30 m. Surface temperatures ranged from -15°C over multiyear ice to -1.7°C over open water. The impact of leads on the upwelling fluxes is seen in Fig. 9 from the coincident low values of upwelling shortwave radiation and the high values of the upwelling longwave radiation. During July, when the sea ice was melting, the surface was very complex (see cover), with open water in leads and the surface meltponds clearly influencing the surface albedo (the hemispheric shortwave radiometers were not capable of resolving the individual small features).

The NASA Ames Solar Spectral Flux Radiometer was deployed on the NASA ER-2, on the UW

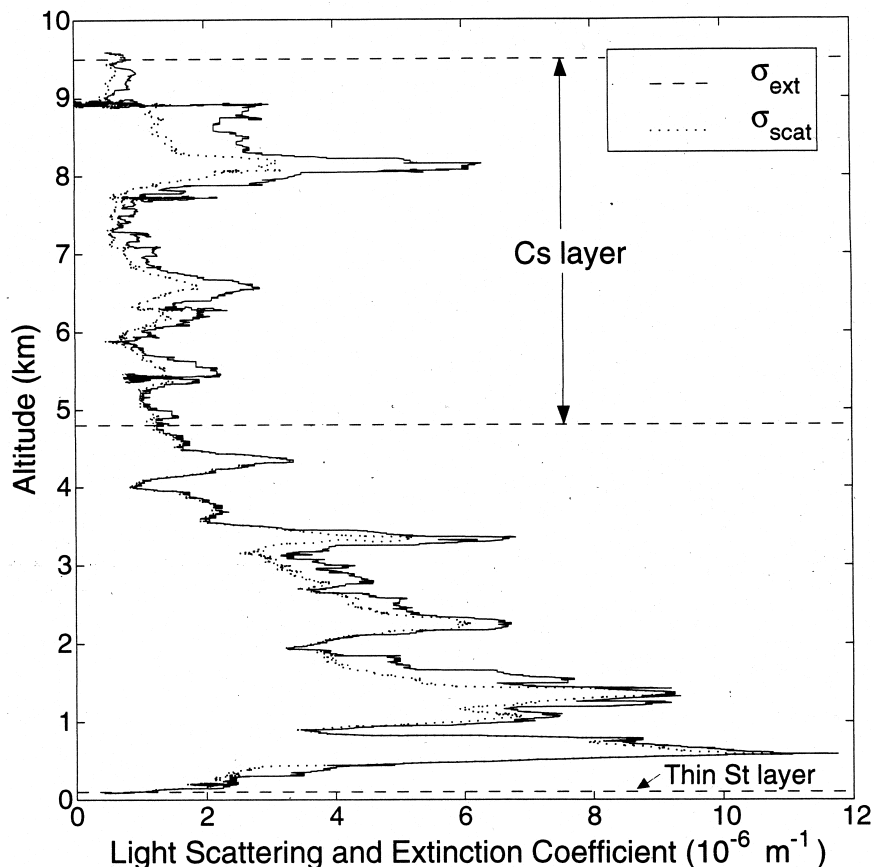


FIG. 7. Vertical profiles of the aerosol light-scattering coefficient, σ_{scat} (dotted line), and the aerosol light-extinction coefficient, σ_{ext} (solid line), at a relative humidity of 30% and a wavelength of 550 nm. The measurements were obtained aboard the UW's Convair-580 aircraft over the Barrow ARM site between 2247 and 2442 UTC on 19 June 1998.

Convair-580, and on the SHEBA ship. Figure 10 shows 22 consecutive hours of spectral downwelling radiance at the SHEBA ship on 15–16 May. Local noon is around 2300 UTC and coincides with maxi-

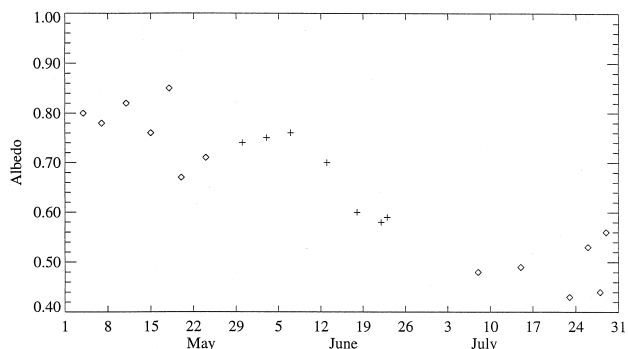


FIG. 8. Time series plot from 4 May through 29 June 1998 of average broadband (300–3000 nm) surface albedos obtained from the C-130Q (May, July) and the UW Convair-580 (June) in the vicinity of the SHEBA ship.

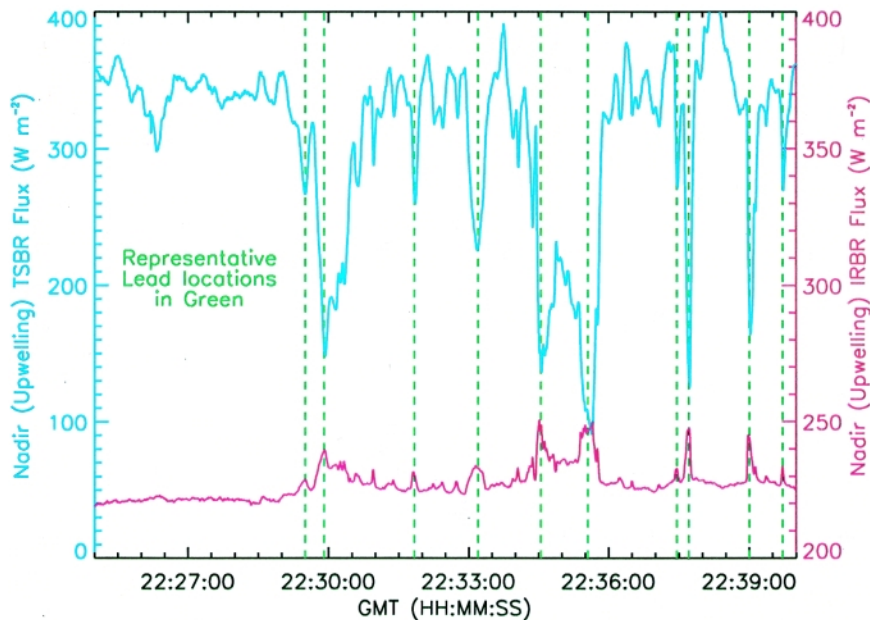


FIG. 9. Time series plot of upwelling longwave (red) and shortwave (blue) radiation obtained by the NCAR C-130 aircraft at an altitude of 30 m on 7 May 1998. The location of leads is indicated in green.

imum signal in clear sky on 15 May; the minimum solar elevation is 6° at approximately 1100 UTC. Before 0300 UTC, water vapor and oxygen features dominate the spectra. By 0400 UTC the effects of cloud are clearly seen by the saturated oxygen band at 762 nm and water vapor band at 940 nm.

homogeneous stratus cloud and for the sea ice surface. Of particular interest in Fig. 11a is the enhanced back-scattering maximum for the stratus cloud that occurs in opposition to the sun. Surrounding this glory feature is a pronounced rainbow (apparent on the left-hand side of Fig. 11a), which is characteristic of water droplet clouds. Figure 11b illustrates the reflection function of sea ice. In contrast to Fig. 11a, sea ice shows no rainbow or glory pattern, and is considerably darker than stratus water clouds at $1.64 \mu\text{m}$ due to the much larger absorption of solar radiation by ice than by water at this wavelength.

The diffuse radiation reflected by arctic stratus clouds and sea ice was measured aboard the UW Convair-580 aircraft while flying a clockwise circular orbit and scanning the scene below the aircraft with the NASA Goddard scanning radiometer (CAR). This radiometer scans at a rate of 100 rpm from zenith to nadir on the starboard side of the aircraft and can map the entire reflection pattern of the surface during a complete circular orbit of the UW Convair-580. With a 1° field of view of the radiometer, a complete bidirectional reflectance distribution function can be obtained for eight wavelengths of the radiometer simultaneously (King 1992). Figure 11 shows the reflectance function of 0.68 and $1.64 \mu\text{m}$ for a

Measurements of cloud optical properties were obtained from a cloud integrating nephelometer, a new instrument flown for the first time on an aircraft (the UW Convair-580) during the FIRE Arctic Clouds Experiment. This instrument is designed for measurements of the asymmetry (g) parameter and optical scattering and extinction coefficients at $0.635 \mu\text{m}$ in liq-

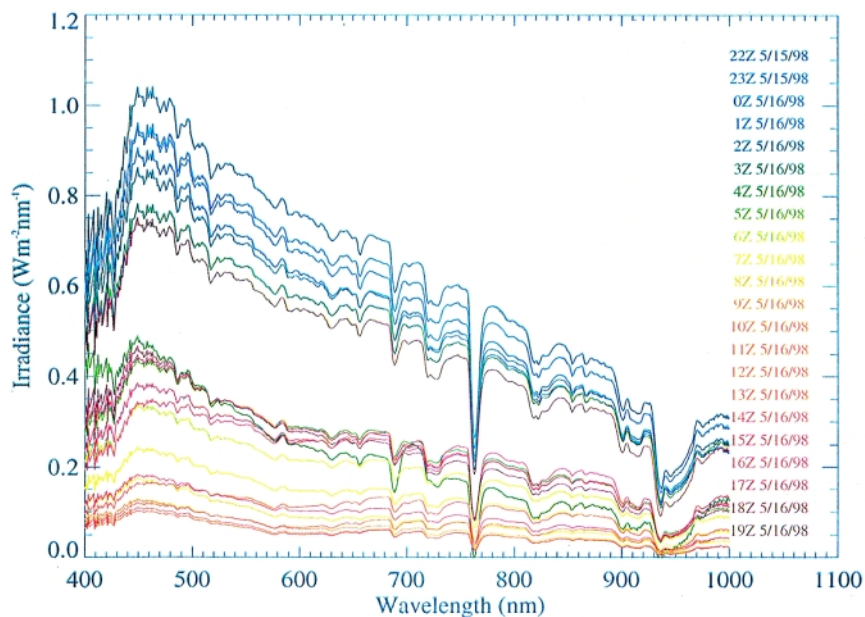


FIG. 10. Observations of spectral downwelling solar irradiance obtained from the Solar Spectral Flux Radiometer at the SHEBA ship on 15–16 May 1998.

uid and ice clouds. An especially interesting case was found on 1 June when the aircraft passed through an ice cloud containing predominantly rosette ice crystals. The optical extinction coefficient and the asymmetry parameter are shown in Fig. 12 for this case. The average-measured asymmetry parameter for this case ($g = 0.715$) is significantly smaller than that found in liquid clouds (with typical values $g = 0.835$).

d. Remote sensing

Remote-sensing data from the NASA ER-2 aircraft are illustrated in Fig. 13 for a case on 20 May near the coast of Barrow. The swath includes tundra covered by snow (and cloud), open water near the coast, and sea ice floes offshore. The ER-2 was flying down the image from top to bottom, encountering single-layer stratus clouds with a cloud-top altitude of around 600 m (CLS). Clouds are readily observed by the MAS at $1.62 \mu\text{m}$ since water clouds are quite reflective at this wavelength, in contrast to open water and sea ice, which are both quite dark at this wavelength (cf. Fig. 11). The MAS visible image ($0.66 \mu\text{m}$) suggests that the clouds were optically thick over the tundra, thinning and becoming semitransparent over the open water. This is also confirmed by examining the vertical cross section of the CLS. The AMPR 37-GHz image clearly shows the surface features, since atmospheric emission at this wavelength is minimal. Open water has low emissivity and hence low brightness temperature at the AMPR frequency of 37 GHz, while snow and ice have high emissivity at 37 GHz and hence appear bright. Comparison of the images at 220 and 37 GHz (MIR) shows that over open water the brightness temperature at 220 GHz is significantly higher because of the higher surface emissivity and significant atmospheric emission at this frequency. Over sea ice, the low brightness tempera-

ture at 220 GHz (but not at 37 GHz) indicates that there is some snow cover on the sea ice, which is detected at 220 GHz because of its shallower penetration depth. This case illustrates the complexity of the polar surfaces and the utility of the combination of visible, near-infrared, submillimeter, and microwave wavelengths in separating out the characteristics of the surface and clouds.

An example of a retrieval of cloud properties from the NOAA-14 AVHRR is shown in Fig. 14 for 2300 UTC 4 May 1998 (corresponding to the case described in Figs. 2–4). The satellite data consists of 1-km AVHRR data taken over the SHEBA Ice Station ($76.0^\circ\text{N } 165.4^\circ\text{W}$). Figure 14a shows the channel 3 ($3.75 \mu\text{m}$) image that depicts a relatively complex cloud system over the area. The data taken in the box

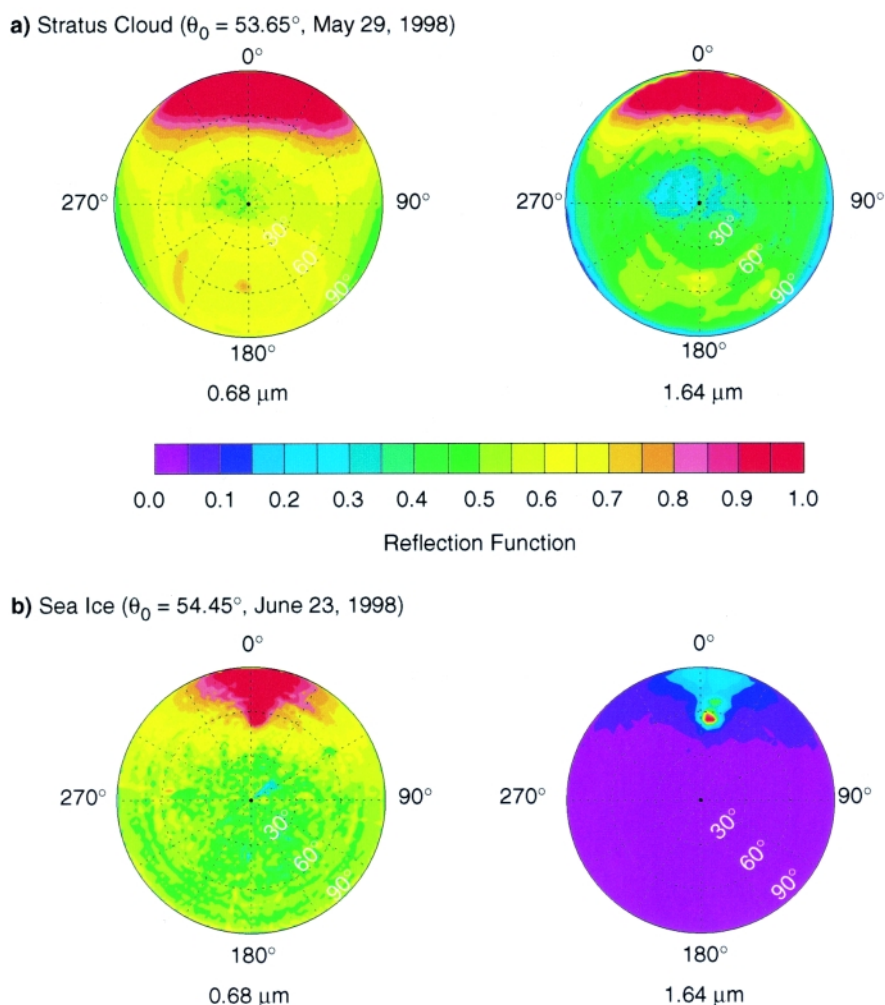


FIG. 11. Bidirectional reflectance function obtained from the Cloud Absorption Radiometer (CAR) on the UW Convair-580 at 0.68 and $1.64 \mu\text{m}$ for (a) homogeneous stratus cloud on 29 May 1998 at $72^\circ 48' \text{N}$, $158^\circ 44' \text{W}$ when the solar zenith angle was 53.65° , and (b) the sea ice surface on 23 June 1998 at $77^\circ 44' \text{N}$, $16^\circ 36' \text{W}$ when the solar zenith angle was 54.45° .

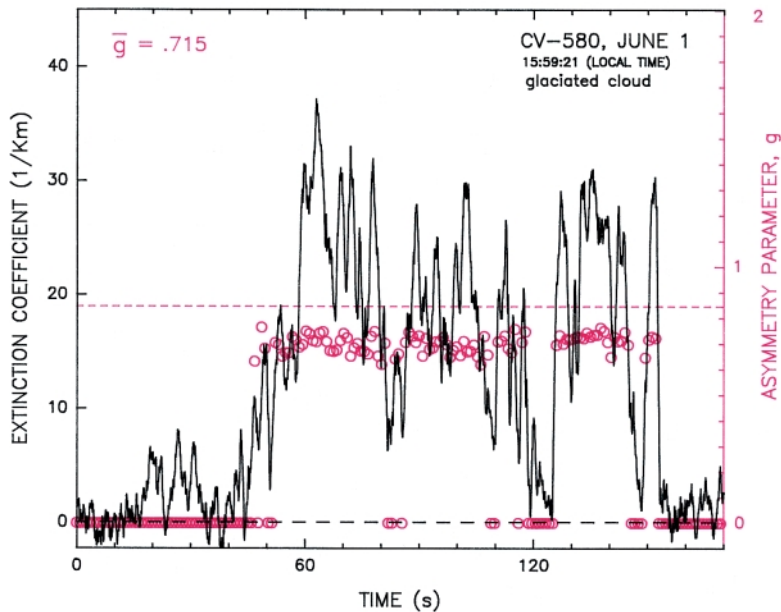


FIG. 12. Time series of the volume extinction coefficient and asymmetry parameter measured with the cloud integrating nephelometer during horizontal flight of the UW's Convair-580 through an ice cloud with $T = -40.5^{\circ}\text{C}$. The red dashed line indicates a typical value of g for a liquid water cloud.

centered over the SHEBA ship (outlined in the satellite image) were analyzed with the solar-infrared, infrared, split-window technique that matches calculations from radiative transfer parameterizations of reflectance and emittance at 3.75 , 10.8 , and $11.9 \mu\text{m}$ to determine cloud phase, particle size, and optical depth for each

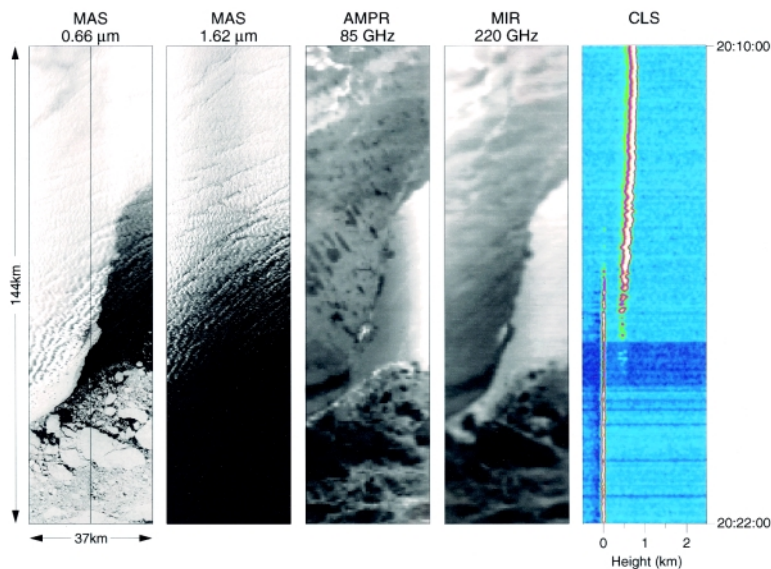


FIG. 13. Composite of observations obtained from the NASA ER-2 aircraft on 20 May 1998 in the vicinity of the Barrow coast. MAS: MODIS Airborne Simulator; AMPR: Advanced Microwave Precipitation Radiometer; MIR: Millimeter-wave Imaging Radiometer; CLS: Cloud Lidar System.

pixel (Minnis et al. 1998). Of the 870 pixels, 18% were classified as liquid water and 82% as ice. The mean effective radius for the water droplets was $6.3 \mu\text{m}$, while the mean effective diameter for the ice crystals was $10.2 \mu\text{m}$. Images of the retrieved particle sizes and optical depths are shown in Fig. 14e. The C-130 in situ instruments observed high concentrations of small, nearly spherical particles near cloud top. Further into the cloud, some liquid water was observed with indications of icing and some drizzle. These observations provide tentative confirmation of the satellite retrievals of cloud particle size and phase. The radar and flight logs, however, show that the retrieved cloud-top altitude is apparently responding to the low concentration of ice crystals between 1 and 3 km.

During July 1998 the NOAA-15 AVHRR became available. This instrument differs from previous AVHRRs because channel 3 measures $1.6\text{-}\mu\text{m}$ radiances during the daylight and $3.75\text{-}\mu\text{m}$ radiances at night. NOAA-15 is the first operational meteorological satellite with the $1.6\text{-}\mu\text{m}$ channel. This spectral band provides extremely good discrimination of snow, clouds, ocean, and land as

shown in the multispectral image in Fig. 15. It is also useful for cloud phase and particle size determination. Snow crystals and water bodies are strong absorbers, so they appear black in the $1.6\text{-}\mu\text{m}$ imagery. Land surfaces are typically more reflective at $1.6 \mu\text{m}$ than at $0.63 \mu\text{m}$ while ice clouds are less reflective than liquid clouds. Thus, the combination of the visible, infrared, and $1.6\text{-}\mu\text{m}$ images shows the cold ice pack as pink, clouds as white, and clear water as deep blue. Thin clouds over the ice indiscernible in either visible or infrared images are quite evident in the $1.6\text{-}\mu\text{m}$ image and multichannel overlay. The new AVHRR data should provide much improved satellite retrievals of cloud properties over the Arctic. The aircraft flights during July 1998 should be quite valuable for validating the interpretation of this new satellite resource.

e. *Single-column modeling*

Data obtained during the FIRE Arctic Clouds Experiment have been used to assess the performance of several large-scale models during May: the European Centre for Medium-Range Weather Forecasts (ECMWF) numerical weather prediction model as it was operational at the time of the experiment, and single-column versions of the Colorado State University (CSU) GCM (Fowler et al. 1996) and the Arctic Regional Climate System Model (ARCSyM) (Pinto et al. 1999). The single-column models are forced with time series of large-scale advective tendencies and divergences obtained from the ECMWF initialized analyses. The surface turbulent fluxes were specified using ECMWF data in the CSU SCM, while turbulent fluxes were modeled in the ARCSyM SCM. The ECMWF column is not allowed to develop its own short-term climate since results are from successive global 12–36-h forecasts; therefore, the simulation is not susceptible to model drift as are the two SCMs described above.

Table 6 shows a preliminary comparison of the monthly averaged values for May of selected cloud and radiation parameters for the ECMWF, CSU, and ARCSyM models against the field observations. The surface radiation fluxes were obtained from a 2-m stand located near the SHEBA ship. Cloud fraction, and base and top heights were determined from the cloud radar and lidar; and cloud liquid water path (LWP) was obtained from the surface-based microwave radiometer. Comparisons of the microwave-derived LWP with that obtained from profiles flown through the cloud layer by the NCAR C-130Q aircraft reveal that the microwave values may be biased toward larger values. Further calibration of the aircraft and mi-

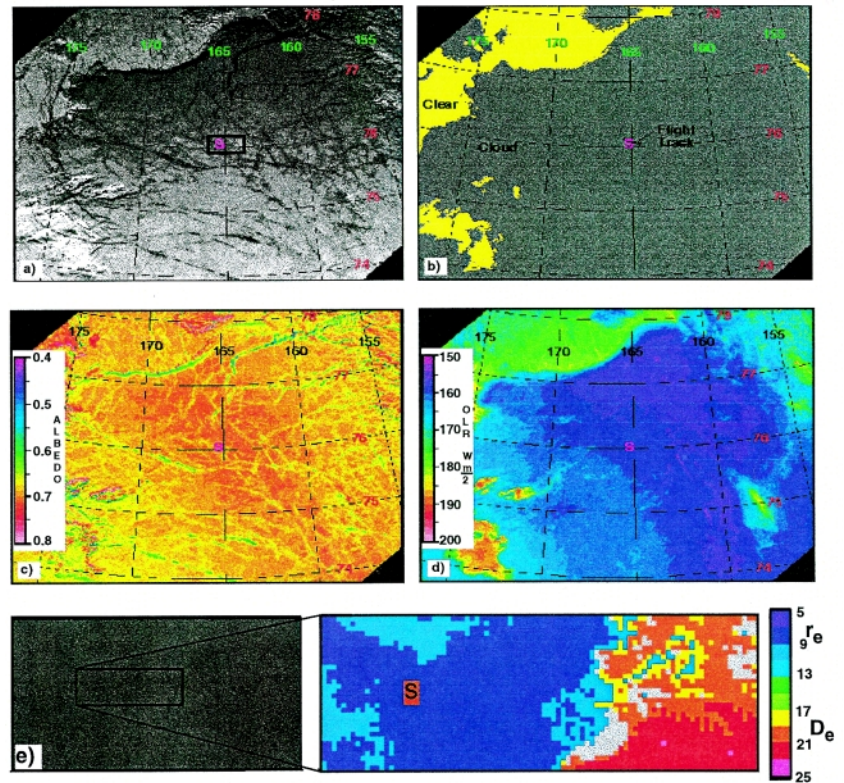


FIG. 14. NOAA-14 AVHRR image and derived cloud radiation products over SHEBA (denoted by “S” in each panel) and the surrounding ice pack at 2252 UTC 4 May 1998. (a) Visible, 1-km resolution image with box outlining area of cloud analysis; (b) cloud mask with coincident C-130Q flight track; (c) broadband shortwave albedo; (d) outgoing longwave radiation in $W m^{-2}$; (e) 3.7- μm image (left panel) and r_e in μm refers to effective radius of cloud liquid water droplets, D_e denotes effective diameter of ice cloud particles; and gray areas indicate that particle sizes could not be retrieved.

TABLE 6. Preliminary comparison of observations (OBS) with model output (ECMWF, ARCSyM, CSU) for a single grid cell centered on the SHEBA ship for the month of May 1998.

| Parameter | OBS | ECMWF | ARCSyM | CSU |
|--|------|-------|--------|------|
| Downwelling longwave radiation ($W m^{-2}$) | 244 | 231 | 227 | 191 |
| Downwelling shortwave radiation ($W m^{-2}$) | 248 | 275 | 291 | 250 |
| Total cloud fraction | 0.82 | 0.69 | 0.51 | 0.89 |
| Liquid water path ($g m^{-2}$) | 43 | 9 | 22 | 13 |
| Cloud-top height (top layer) (km) | 3.3 | 3.8 | 3.2 | 6.9 |
| Cloud-base height (bottom layer) (km) | 1.2 | 0.8 | 0.5 | 1.9 |

crowwave data should bring these observations closer together.

The ECMWF and ARCSyM models significantly underpredict the total cloud fraction. Cloud fraction estimates obtained individually from the lidar and radar differ by a few percentage points, but this discrepancy is small relative to the discrepancies with the model simulations. The ECMWF model is fairly successful at reproducing the observed cloud heights. Although the total cloud fraction modeled by CSU agrees well with the observations, the model appears to produce more high clouds and fewer low clouds than observed. All three models substantially underpredict the LWP.

The errors in the modeled cloud properties contribute to the biases in the surface radiative fluxes. ECMWF and ARCSyM models predict surface downwelling shortwave radiation fluxes that are too large and surface downwelling longwave radiation fluxes that are too small, which is consistent with model underprediction of cloud fraction and liquid water

path. The CSU CSM reproduces very well the downwelling shortwave radiation flux but the downwelling longwave radiation flux is substantially underestimated, which is consistent with the predominance of high clouds simulated by this model.

Further details of the intercomparison of the observations with the SCMs are shown in Fig. 16 for the time series of cloud LWP and surface radiation fluxes. It is seen that cloud events in both models are either missed (16–19 May) or the LWP of the modeled clouds is underpredicted. The underprediction of LWP is partly associated with inaccurately representing cloud layers as crystalline. As seen on 12 May, the underpredicted LWP may result in a large error in the modeled net shortwave flux but small errors in the downward longwave flux. Missed cloud events result in gross errors in both the downwelling longwave and net shortwave radiation, as seen on 29 May. The first 10 days of both simulations are characterized by low liquid clouds that occur in a layer with a significant warm

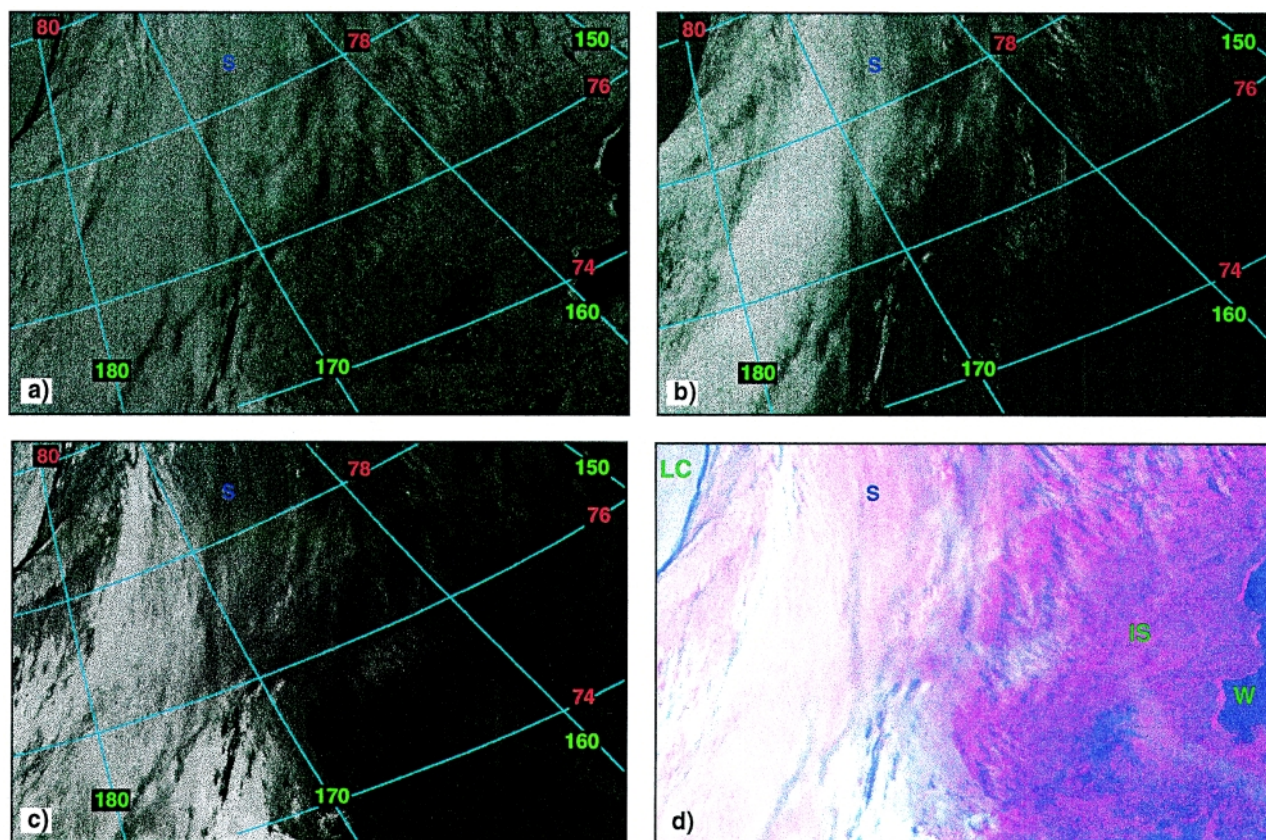


FIG. 15. NOAA-15 AVHRR 1-km imagery at 2021 UTC 26 July 1998 over the Arctic Ocean. The location of the SHEBA ship is denoted with an “S.” (a) 0.63- μm image; (b) 11- μm image; (c) 1.6- μm image; and (d) pseudo-color image with red, green, and blue intensities determined by the 0.63- μm reflectance, 1.6- μm reflectance, and the reversed 11- μm temperature (snow: pink, open water: dark blue, thick water cloud: white, ice clouds: light blue-gray).

bias that is associated with the large-scale forcing supplied by ECMWF; hence, when clouds with significant LWP are simulated, the downwelling longwave radiation is substantially overestimated. The “clear-sky” radiative transfer in the ARCSyM SCM is handled fairly well while larger clear-sky biases are evident in the CSU GCM (as indicated by 22–25 May in Fig. 16). The modeled clear-sky downwelling solar flux is too large in both models around solar midnight. This could be the result of problems with the plane-parallel approximation at high zenith angles. The radiative impact of aerosols, which has not been included in these models, may also contribute to the bias seen in the net solar flux at the surface.

6. Conclusions

The FIRE Arctic Clouds Experiment successfully met its operational objectives, namely to conduct a multi-aircraft study of clouds and radiation over the Arctic Ocean in the vicinity of the SHEBA ice station and the ARM Barrow site. The overall design of the experiment was to combine measurements at the surface, from research aircraft, and from space to address problems of arctic clouds, radiation, and aerosols, including their modeling and remote sensing. The complex experimental design was judged to be very successful in terms of its efficiency, economy, and completeness.

Preliminary analysis of the data indicates that the dataset contains a wealth of information on clouds, radiation, and aerosol to address the scientific questions, remote sensing issues, and modeling objectives of the project. Preliminary scientific highlights that illuminate the science questions presented in section 2 include the following:

- A persistent humidity inversion above boundary layer cloud tops, associated with the static stability of the arc-

tic environment, contributes to the homogeneity and persistence of the cloud by inhibiting evaporative cooling associated with entrainment mixing at cloud top.

- Evidence was found of direct association of low-level clouds with open water in polynyas.
- Large variations in the relationship between cloud temperature and phase were found, influenced by the presence of ice nuclei, seeding of the cloud by ice particles falling from above, and the size of the liquid drops.
- Aerosol composition is commonly highest aloft, especially during spring, associated with long-range transport and scavenging in the lower atmosphere by boundary layer clouds. Local production of aerosols was observed in dissipating cloud layers, the humidity inversion, and was associated with local production of dimethyl sulfide.
- There is some evidence that the open water in leads may provide a source of ice forming nuclei.
- Direct evidence was given for the susceptibility of

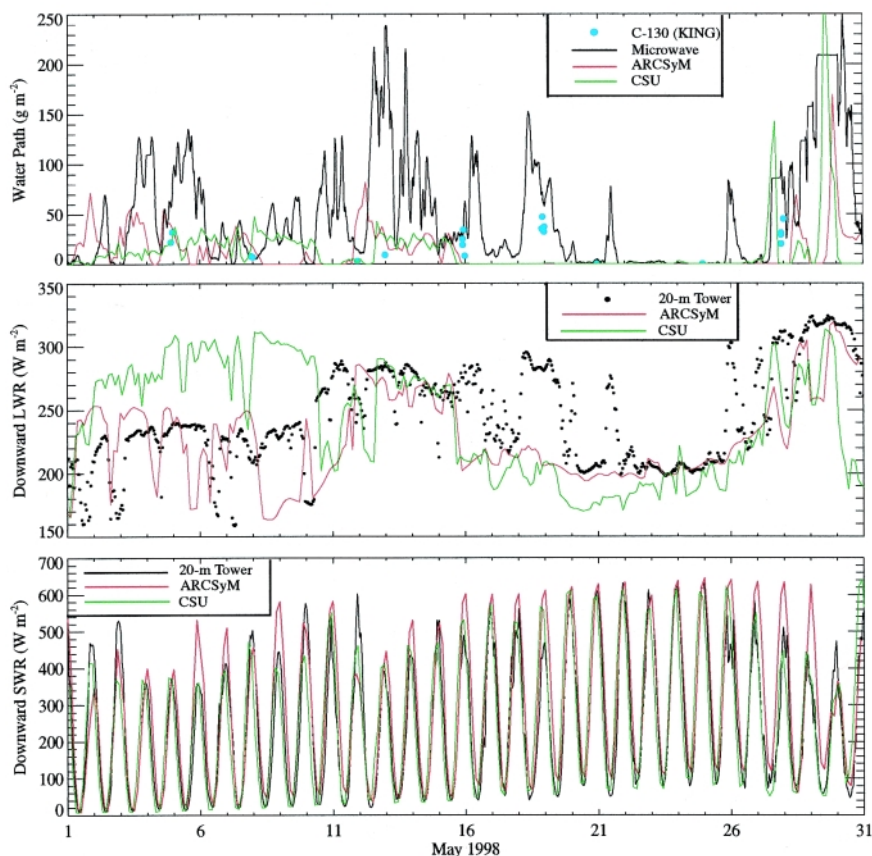


FIG. 16. Comparison of simulations of the ARCSyM and CSU single-column models with SHEBA observations during the month of May: (top) liquid water path; (middle) downwelling surface longwave radiation; (lower) net surface shortwave radiation.

arctic cloud microphysical and optical properties to modification by anthropogenic aerosol.

- The spatial inhomogeneity of the surface physical and optical characteristics is very large, especially during the summer melt season. Temporal variations in surface albedo were documented to occur in response to atmospheric forcing: the first seasonal rainfall markedly decreased the snow surface albedo and heralded the onset of snowmelt; substantial variations (up to 20%) in surface albedo arose from variations in cloud optical depth that were not associated with any variations in surface characteristics; and late summer surface albedo changes occurred in response to freezing and thawing of the surface in response to storms.
- Measurements of the asymmetry parameter show the substantial effect that habit and size of the ice crystals have on the radiative transfer.
- The combination of visible, near-infrared, sub-millimeter, and microwave wavelengths shows considerable promise in discriminating the characteristics of the surface and clouds under many conditions that have hitherto been difficult to identify using only a single sensor.
- The ECMWF, CSU, and ARCSyM models tend to underpredict low cloud amount and the column liquid water path, resulting in simulations of surface net shortwave radiative fluxes that are too large, and downwelling longwave radiative fluxes that are too small.

Our initial assessment of the dataset indicates that it will provide the basis for definitive answers to some of the science questions articulated for the project, and progress toward addressing the others. Preliminary single-column modeling studies indicate that considerable work needs to be done to assess and minimize the impact of uncertainties in the boundary advection, but significant progress is already being made in developing and testing new parameterizations using this dataset. The dataset is already being used to evaluate satellite cloud and sea ice retrievals and is forming the basis for improved satellite remote sensing algorithms using multiple sensors.

Ultimate achievement of the full objectives of the FIRE Arctic Clouds Experiment will require extensive analysis of the data and comparison with models and satellite retrievals by many scientists, both within and beyond the FIRE Science Team. To facilitate collaboration, the datasets are being archived in a form that will make them readily accessible worldwide.

Further information on the FIRE Arctic Clouds Experiment and data archival can be found at http://eosweb.larc.nasa.gov/ACEDOCS/ace_intro.html and <http://ltpwww.gsfc.nasa.gov/MAS/FIREIII.pdf>.

Acknowledgments. The FIRE Arctic Clouds Experiment was funded by the National Aeronautics and Space Administration, National Science Foundation, Department of Energy, Environment Canada, the Canadian National Research Council, and the Canadian Panel on Energy Research and Development. We would like to thank the following individuals and groups who helped make this experiment a success: D. McDougal and the FIRE Project Office, K. Laursen and the staff of the NCAR Research Aviation Facility, the flight crews of the University of Washington and Canadian Convair-580s, the U.S. Army at Fort Wainwright, the Geophysical Institute at the University of Alaska, the NASA Langley Research Center DAAC and Communications and Computer Systems Branch, scientists and technical personnel on the *Des Groseilliers*, and all of the scientists, students, and technical personnel who participated in the field experiment. We are grateful to the ECMWF for providing a special assimilated dataset for the single-column model experiments. We would like to also thank R. Hood, J. Wang, J. Spinhirne, the ARM program, and the SHEBA Project Office for contributing data to this paper. Comments from the anonymous reviewers significantly improved the presentation of the paper. Members of the FIRE Arctic Science Team are C. Bretherton, W. Cotton, J. Curry, A. Del Genio, W. Eberhard, C. Fairall, H. Gerber, J. Hallett, C. Jakob, P. Hobbs, J. Hudson, G. Isaac, M. King, Y. Kogan, S. Kreidenweis, S. Krueger, P. Lawson, D. Lenschow, M. Miller, P. Minnis, P. Pilewskie, D. Randall, W. Rossow, J. Spinhirne, S. Tsay, T. Uttal, F. Valero, S. Wang, Q. Wang, B. Wielicki, and D. Wylie.

References

- Benoit, R., M. Desgagne, P. Pellerin, Y. Chartier, and S. Desjardins, 1997: The Canadian MC2: A semi-Lagrangian semi-implicit wideband atmospheric model suited for finescale process studies and simulation. *Mon. Wea. Rev.*, **125**, 2382–2415.
- Curry, J. A., W. B. Rossow, D. Randall, and J. L. Schramm, 1996: Overview of Arctic cloud and radiation properties. *J. Climate*, **9**, 1731–1764.
- Ferek, R. J., P. V. Hobbs, L. F. Radke, J. A. Heering, W. T. Sturges, and G. F. Cota, 1995: Dimethyl sulfide in the arctic atmosphere. *J. Geophys. Res.*, **100**, 26 093–26 104.
- Fowler, L. D., D. A. Randall, and S. A. Rutledge, 1996: Liquid and ice cloud microphysics in the CSU general circulation model. Part I: Model description and simulated microphysical processes. *J. Climate*, **9**, 489–529.
- Hobbs, P. V., and A. L. Rangno, 1998: Microstructures of low- and middle-level clouds over the Beaufort Sea. *Quart. J. Roy. Meteor. Soc.*, **124**, 2035–2071.
- King, M. D., 1992: Directional and spectral reflectance of the Kuwait oil-fire smoke. *J. Geophys. Res.*, **97**, 14 545–14 549.
- Minnis, P. D., P. Garber, D. F. Young, R. F. Arduini, and Y. Takano, 1998: Parameterization of reflectance and effective

- emittance for satellite remote sensing of cloud properties. *J. Atmos. Sci.*, **55**, 3313–3339.
- Perovich, D. K., and Coauthors, 1999: Year on ice gives climate insights. *Eos, Trans. Amer. Geophys. Union*, **80**, 481.
- Pinto, J. O., J. A. Curry, and A. H. Lynch, 1999: Modeling clouds and radiation for the November 1997 period of SHEBA using a column climate model. *J. Geophys. Res.*, **104**, 6661–6678.
- Randall, D. A., B. A. Albrecht, S. K. Cox, P. Minnis, W. Rossow, and D. Starr, 1995: On FIRE at ten. *Advances in Geophysics*, Vol. 38, Academic Press, 37–177.
- , K.-M. Xu, R. J. C. Somerville, and S. Iacobellis, 1996: Single-column models and cloud ensemble models as links between observations and climate models. *J. Climate*, **9**, 1683–1697.
- , and Coauthors, 1998: Status of and outlook for large-scale modeling of atmosphere–ice–ocean interactions in the Arctic. *Bull. Amer. Meteor. Soc.*, **79**, 197–219.
- Stokes, G. M., and S. E. Schwartz, 1994: The Atmospheric Radiation Measurement (ARM) program: Programmatic background and design of the cloud and radiation test bed. *Bull. Amer. Meteor. Soc.*, **75**, 1201–1221.

